Invited paper

Tide distribution and tapping into tidal energy

OCEANOLOGIA, 46 (3), 2004.
pp. 291–331.

KEYWORDS
Tides
Extreme tides
Energy conservation
Tidal power plants

Zygmunt Kowalik

Institute of Marine Science,
University of Alaska,
Fairbanks, AK, 99775, USA;

e-mail:ffzk@ims.uaf.edu

Manuscript received 17 June 2004, reviewed 30 July 2004, accepted 19 August 2004.

Abstract

Tidal power along tidal shores has been used for centuries to run small tidal mills. Generating electricity by tapping tidal power proved to be very successful only in the last century through the tidal power plant constructed in 1967 in La Rance, France. This used a large barrier to generate the sea level head necessary for driving turbines. Construction of such plants evolved very slowly because of prohibitive costs and concerns about the environmental impact. Developments in the construction of small, efficient and inexpensive underwater turbines admit the possibility of small scale operations that will use local tidal currents to bring electricity to remote locations. Since the generation of such electricity is concerned with the tidal energy in local water bodies, it is important to understand the site-specific energy balance, i.e., the energy flowing in through open boundaries, and the energy generated and dissipated within the local domain. The question is how to tap the tidal energy while keeping possible changes in the present tidal regimes to a minimum. The older approach of constructing barrages may still be quite useful in some locations. The basics of such tidal power plants constructed in a small bay are analyzed in order to understand the principal parameter for tidal plant evaluation, i.e., the power produced.

The new approach is to place turbines – devices similar to windmills – in the pathway of tidal currents. Theoretically, the amount of power available by such turbines for electricity generation is proportional to the water density and velocity

cubed of the tidal flow. The naturally dissipated tidal power due to bottom friction forces is also proportional to the cube of the velocity. Because of this similarity, the exploitation of tidal energy can be directed to reinvesting the naturally dissipated power into tidal power for the generation of electricity. This approach to tidal power exploitation is better tuned towards preservation of the natural tidal regime.

To answer the many questions related to tidal regime changes, it is important to develop a new branch of tidal dynamics which will help to better understand the interaction between a natural tidal regime and future changes caused by tapping into tidal energy.

1. Introduction

At present, tidal power plants (TPP) use both potential (tidal sea level) and kinetic energy (tidal currents). Both uses have their roots in the small tide mills constructed along tidal shores. In a tidal mill, a small pond is connected to the open ocean through a sluice. During flood tides a gate in the sluice is lowered so that the pond is filled up with incoming water. This water is stored in the pond until the ebb tide, when the gate is raised and the water head generated is applied to move a waterwheel (Bernshtein 1961). Since modern tidal plants tap both potential and kinetic energy, a knowledge of tide distributions in the World Ocean is critical to the development of tidal power on a site-specific basis. To illustrate the basic tidal physics governing the large tidal levels, a few locations with very large tides have been singled out. While tidal sea levels are quite easy to understand and predict, tidal currents are less amenable to investigation. Currents are strongly modified by the local bathymetry and shoreline geometry. Strong flows occur in relatively shallow water and in constrained passages. Tides change in density-stratified waters by generating internal tides which locally enhance tidal currents (Wunsch 1975). Exploitation of tidal energy is usually restricted to limited sites that display a large range of tidal elevations, or strong tidal currents, or both. Consequently, it is important to understand the balance of the tidal energy at such sites. This balance includes accounting for the energy inflow and outflow to and from the local domain, and the sources and sinks of energy within the local domain (Nekrasov 1992, LeProvost & Lyard 1997). An example of the energy balance approach is discussed for the Sea of Okhotsk, where one of the largest tidal ranges has been recorded (13.9 m) in the Penzhinskaya Guba.

Potential energy generated by sea level difference has been used to produce electricity through the construction of barrages to dam water passages, so that the water head necessary for turbine operation can be established. The knowledge for such constructions has been achieved mainly through the investigations of French scientists and engineers, and was

implemented in the 240 MW TPP at La Rance, Brittany, France, in 1967 (Gibrat 1966). The power plant taps tidal energy during a limited time period when the sea level difference between the basin and the open ocean is large enough to drive the turbines. A simple consideration based on the conservation of volume connects the power thus generated to the sea level changes in the basin and the discharge through the dam.

The older use of tidal power by blocking the entrance to a bay with a dam was implemented very slowly, because of the prohibitive costs of such a construction. The new approach is to use tidal currents in a way similar to that in which windmills are used to tap wind energy. This relatively inexpensive method is stimulating tidal power development and has the potential to provide large amounts of energy (Garrett & Cummins 2004). A simple theory shows that the maximum power available from the moving fluid is proportional to the fluid density times the velocity cubed. Because the density of sea water is approximately 900 times greater than that of air, the same amount of energy generated by a wind can be achieved by a relatively much slower water movement.

2. The short description of tides in the World Ocean

The distribution of the tidal amplitude and phase in the World Ocean based on Topex/Poseidon satellite observations and on global numerical models has been summarized by Shum et al. (1997), with the final products recorded on a diskette entitled *A Collection of Global Ocean Tide Models*, available at email: podaac@podaac.jpl.nasa.gov. In Figs 1–4 the charts of amplitude and phase of the four major tidal constituents (M_2, S_2, K_1 and O_1) are shown based on satellite observations. The data and figures were compiled by G. Musiela from The National Tidal Facility (NTF), Adelaide, Australia. To simplify the description, reference will often be made to the M_2 tide – the semidiurnal constituent due to the moon's attraction a period equal to half of the mean lunar day. This is the strongest constituent in the entire spectrum of tidal oscillations. The tide producing force at this frequency is twice as strong as that for the K_1 tide, the major diurnal constituent (Pugh 1987).

It is useful to notice that in the charts the same color denotes the different amplitudes for the different constituents. Both M_2 and K_1 waves in the Pacific and Atlantic Oceans propagate around amphidromic points, where the amplitude of the tidal wave is close to zero. According to the simple long wave dynamics represented by a Kelvin wave propagating in a wide channel, counterclockwise rotation is expected in the northern hemisphere and clockwise rotation in the southern hemisphere (Taylor 1921, Pugh 1987, Godin 1988). As can be seen in the figures, not all waves in

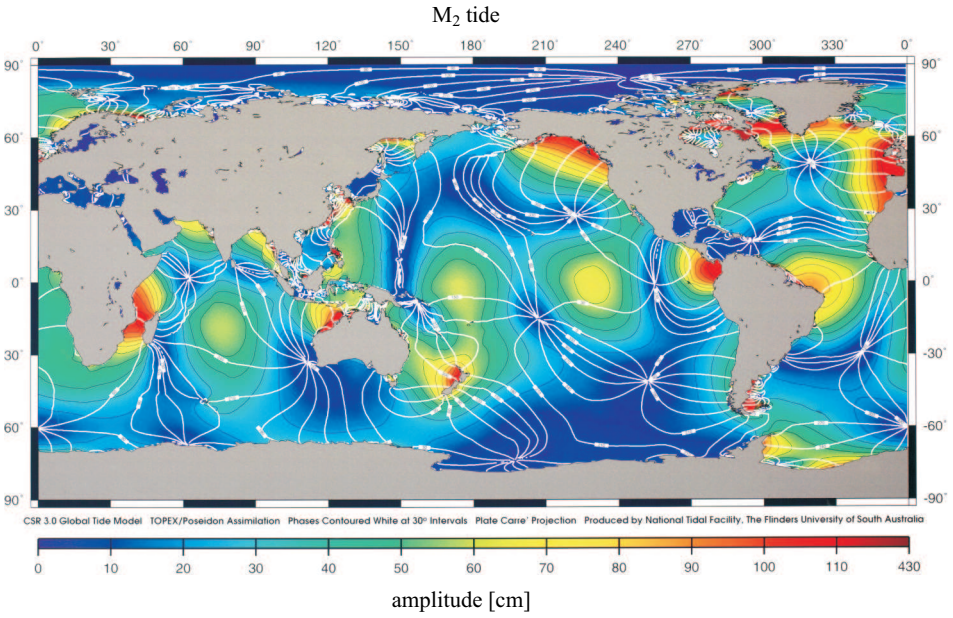

Fig. 1. M_2 tide in the World Ocean. Amplitude (dark lines) is given in cm and phase (white lines, degree) is referred to Greenwich. Courtesy of G. Musiela, NTF, Australia

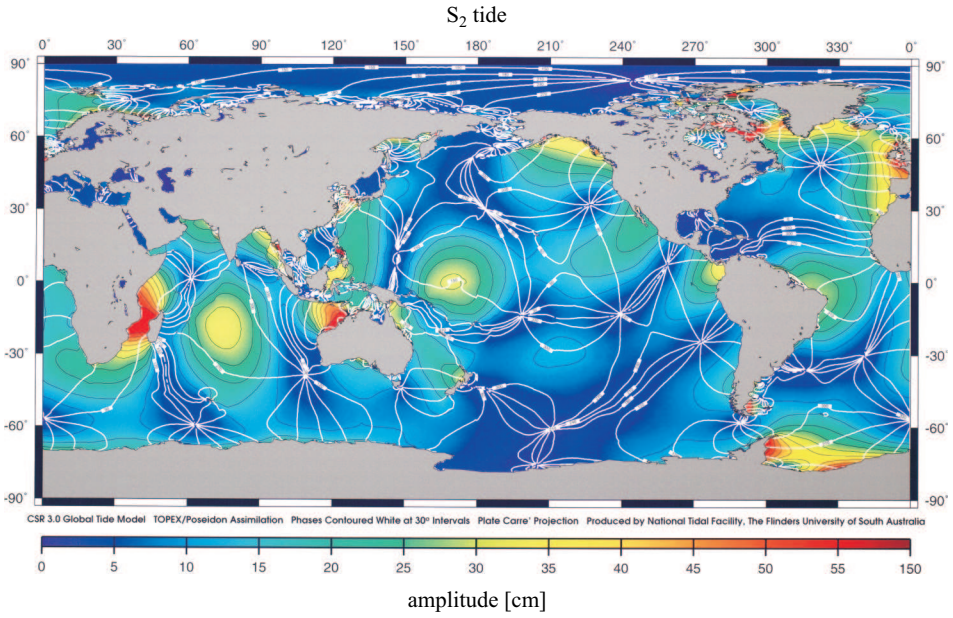

Fig. 2. S_2 tide in the World Ocean. Amplitude (dark lines) is given in cm and phase (white lines, degree) is referred to Greenwich. Courtesy of G. Musiela, NTF, Australia

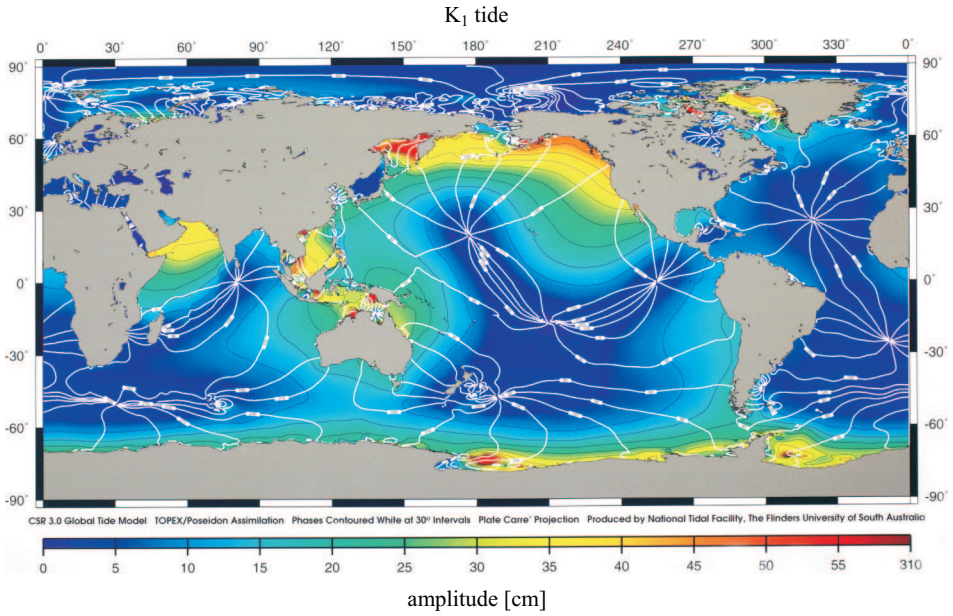

Fig. 3. K_1 tide in the World Ocean. Amplitude (dark lines) is in cm and phase (white lines, degree) is referred to Greenwich. Courtesy of G. Musiela, NTF, Australia

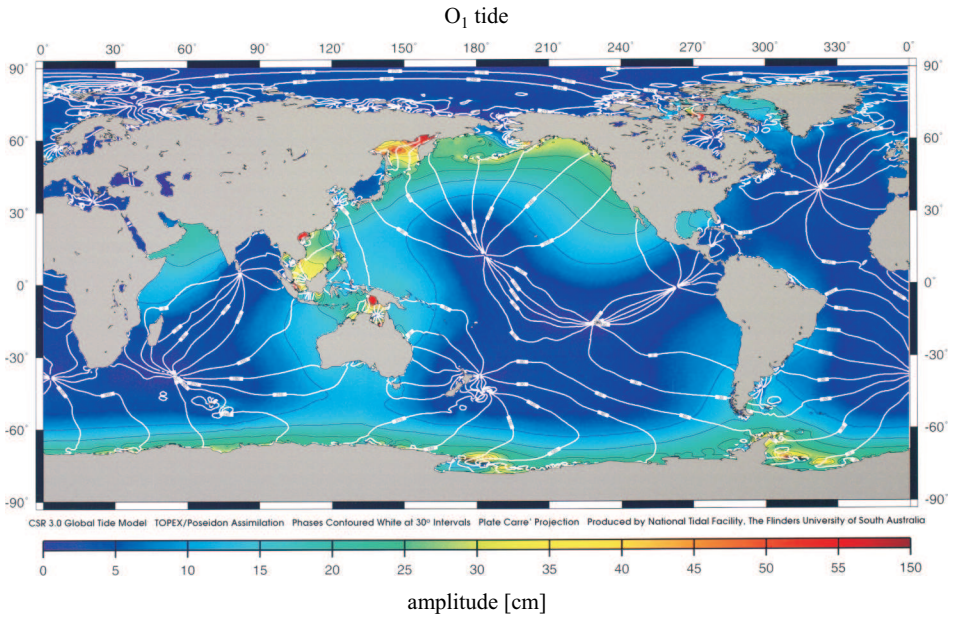

Fig. 4. O_1 tide in the World Ocean. Amplitude (dark lines) is in cm and phase (white lines, degree) is referred to Greenwich. Courtesy of G. Musiela, NTF, Australia

the Pacific and Atlantic Oceans rotate according to the expected patterns. Color coded amplitudes filter out the locations of the higher tidal amplitudes in the World Ocean. The largest surface area covered by the red color for the semidiurnal tides is observed in the north-eastern Atlantic Ocean off the coasts of north-west Africa, western Europe and Greenland. The amplitudes of the semidiurnal tides are also high around South America in the Amazon Basin and off southern Argentina. The largest surface area of the relatively high semidiurnal tides in the Pacific Ocean occurs in the Gulf of Alaska, off equatorial South America and around New Zealand. Other regions with high semidiurnal tides are located off western Australia and between Madagascar and Africa.

Diurnal tides, as expressed by the K_1 wave, have relatively large amplitudes in the North Pacific, with the largest surface area covered by red and yellow-red colors in the Gulf of Alaska and the southern part of the Bering Sea, but these amplitudes are much smaller than the M_2 amplitude. The highest diurnal tides have been recorded in the Sea of Okhotsk. Stronger diurnal tides also occur in the Persian Gulf, the Java Sea, the west coast of New Guinea, and off northern Australia and Antarctica. The diurnal tide distribution contrasts with the semidiurnal tide distribution: while semidiurnal waves depict maxima both in the open ocean and in coastal regions, diurnal waves are very small in the open ocean and their amplitude grows only close to the continents.

To describe the total tidal range we shall use the largest observed tidal range, defined as the mean spring range (Pugh 1987). In the open ocean the tidal range is about 0.5–1 m. The change of depth and coastline has a strong influence on the tidal amplitude (and an even stronger one on the tidal current). Generally along oceanic coasts the tidal range is less than 1.5–2 m. Tidal ranges exceeding 5–6 m have been observed only in narrow bays or channels where the depth changes quite smoothly from the mouth to the head (cf. Defant 1960, Godin 1988).

Usually, the bays with large tides, like the Bay of Fundy on the Atlantic coast of North America, the White Sea in the Northern Russia, Penzhinskaya Guba in the Sea of Okhotsk or Cook Inlet in the Gulf of Alaska, exhibit amplification of the tide that occurs from the mouth to the head of the bays. Such tidal patterns may be attributed either to the gradual shallowing and narrowing of the bay or resonance condition, when the natural period (eigenperiod) of oscillations of the bay is close to the tidal period (Defant 1960).

This brief description of tides is aimed to delineate the locations with high tidal ranges for possible tidal power exploitation. Along with the potential energy expressed by the tidal range, the kinetic energy expressed

by the current can be used as well. Construction of charts for tidal currents is quite difficult, because currents display strong spatial variability. The general oceanic tidal models (cf. LeProvost et al. 1994, Kantha 1995, Shum et al. 1997) calculate the distribution of currents as well, but the spatial grid applied in such calculations (20–40 km) is not adequte for small-scale resolution. Therefore, we will mention here a few important properties of tidal currents. Obviously, a high tidal range generates large currents, but relatively strong currents can be generated by coastal and bathymetric constraints even if tidal elevations are small. The most conspicuous topographic enhancement of tidal flow occurs in Cook Inlet, Alaska, where the M_2 tide current increases up to 3–4 m s^{-1} (Patchen et al. 1981, US Coastal Pilot 1995). This current enhancement is related to large tides, whose range is close to 10 m. On the other hand, in the passages between the Aleutian Islands, strong currents of the order of 2.5–3 m s^{-1} are not associated with high tides because the tidal range there is only about 1 m.

Semidiurnal and diurnal tidal currents sometimes behave similarly, but are often different. Tides propagating from the deep ocean onto the continental shelf change velocity because of changes in the bathymetry. The shelf break also induces a strong vertical motion and, in a stratified ocean, large-amplitude internal tides are generated as well. These waves can give rise to large currents but they do not influence the sea level. Large-amplitude internal wave packets are often observed in the shelf break region (Holloway 1987). All tidal waves impinging on the shelf break become slightly deformed and additionally, in mid-latitudes, diurnal tides are also selectively trapped in the shelf break region. Resonance in the diurnal band of oscillation can generate an enhanced current and trap tidal energy away from the shelf domain as well. Trapped diurnal tidal waves often occur at the edges of continental shelves, in canyons and over seamounts (Cartwright 1969, Kowalik & Proshutinsky 1993). This trapping of diurnal tides by the local bathymetry leads to enhancement of tidal currents, while the change in sea level is quite small. Over the shelf and in shallow bays, in the passages between islands, close to headlands and around banks the tidal currents, both in the diurnal and semidiurnal band of oscillations, can be strongly amplified, which often leads to strong nonlinear interactions.

3. Short description of extreme tide ranges

There now follows a brief description of the highest tides in a few locations of the World Ocean. Although the tidal constituents (amplitude and phase) are constant, the resultant tides depend on many time-dependent factors which tend to generate variable sea level elevations. The highest tidal ranges given below are expected to occur at least once per year.

The Bay of Fundy. Tidal range 17 m. The bay is located on the Atlantic coast of Canada and has the highest tides recorded in the World Ocean. Tides in the bay are dominated by semidiurnal oscillations with high waters and low waters each approximately of the same range. The high tides have been attributed to the fact that the natural period of the Gulf of Maine – Bay of Fundy system is close to, but slightly above, the M_2 period (Garrett & Greenberg 1977, Greenberg 1979). The evidence for this comes from an examination of the tidal amplification at the various ports as a function of the frequency and existence of the highest amplification peak at the M_2 frequency. In the Bay of Fundy proper the amplitude of M_2 tides changes from approximately 2 m at the entrance to more than 5 m in Minas Basin and to more than 4.5 m in Chignecto Bay (see Fig. 5). Along with the high tides, strong tidal currents occur which can also be used for tidal power generation. The half-flood tide currents along the south shore of the Bay of Fundy are close to 100 cm s^{-1} and along the north shore about 75 cm s^{-1}. The obvious locations for the strong currents are narrow passages like Cape Split, dividing Minas Channel from Minas Basin; here the maximum flood tide current is close to 4 m s^{-1}. Flood tides entering rivers cause strong currents and bores. The Saint John River empties through a shallow sill about 4 m deep; tides here cause a strong current alternating in direction, known as 'reversing falls'. Strong tides and narrow passages seem to be

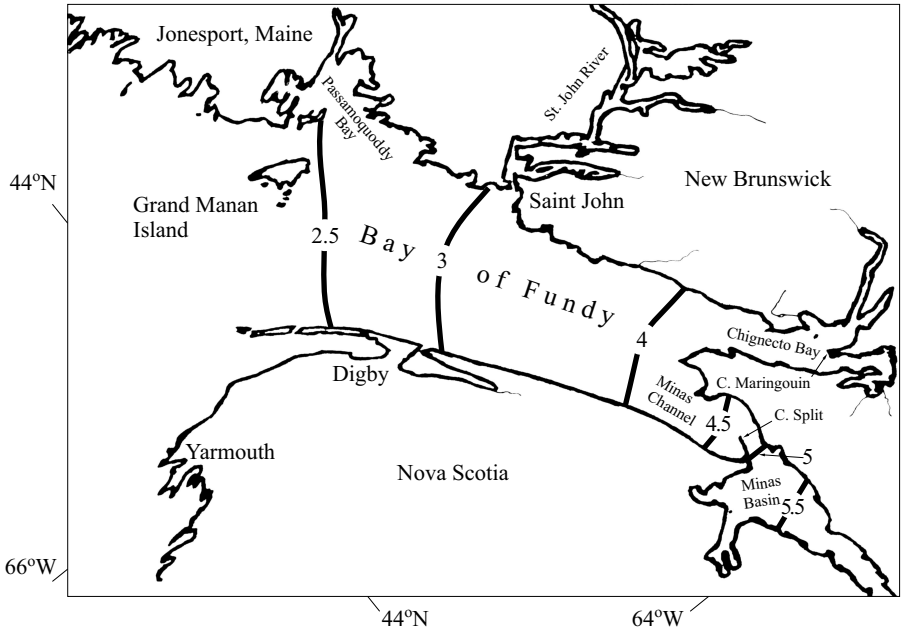

Fig. 5. Amplitude (in meters) of the M_2 tide in the Bay of Fundy

ideal for tidal power utilization, therefore, in the Bay of Fundy a small pilot plant for tidal power generation has been constructed at Annapolis Royal, Nova Scotia. The mean tidal amplitude of the M_2 tide at this site is more than 3 m.

Penzhinskaya Guba. Tidal range 13.9 m. This bay is located in the north-eastern part of the Sea of Okhotsk (Fig. 6). The Sea of Okhotsk's natural period of oscillations is close to 26 h, therefore the diurnal tides are resonantly enhanced and dominate the semidiurnal tides. Both M_2 and K_1 waves are generated by tides entering the Sea of Okhotsk through the passages between the Kuril Islands, and both tides show a similar amplitude in the North Pacific. The Shelikhov Bay – Penzhinskaya Guba system amplifies all the tidal waves. At the entrance to Shelikhov Bay the K_1

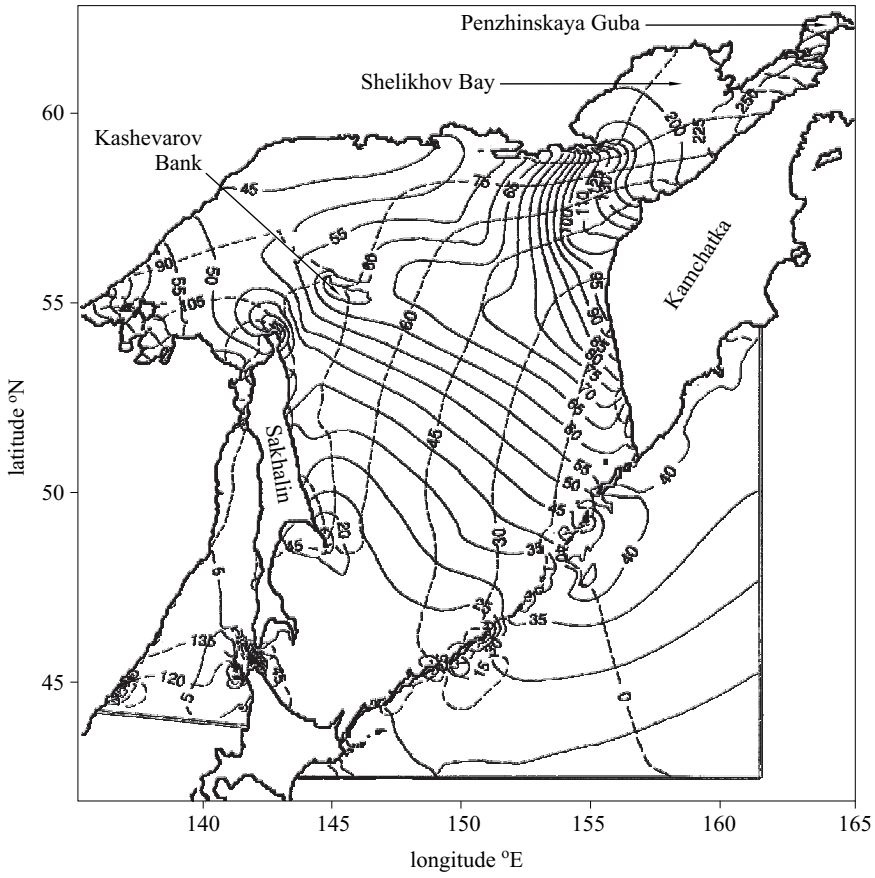

Fig. 6. Amplitude and phase of the K_1 tide in the Okhotsk Sea based on Kowalik & Polyakov (1998). The amplitude (solid lines) is in cm and the phase (dashed lines, degree) is referred to Greenwich

wave amplitude is close to 150 cm, O_1 is about 100 cm and M_2 is 50 cm. While K_1 is amplified to about 250 cm (about two times), K_1 to about 180 cm (about two times) and M_2 to about 120 cm, thus suggesting that the system of Shelikhov Bay and Penzhinskaya Guba is better tuned to the semi-diurnal periods.

An interesting and important phenomenon for tidal power exploitation is diurnal tide trapping, i.e. a region where tidal currents are enhanced. This phenomenon is also known as a tidally induced trapped shelf wave. Because tidal frequencies ω straddle the local Coriolis frequency, diurnal and semidiurnal constituents have different tidal wave dynamics for a given Coriolis force, gravity, and bathymetry. In particular, in the Sea of Okhotsk, diurnal tides are subinertial and semidiurnal tides are superinertial. The inertial frequency ($\omega = f$, where $f = 2\Omega \sin\phi$, Ω is the Earth's rotation frequency and ϕ is the geographical latitude), separates different types of wave motions: gravity forces determine wave behavior at $\omega > f$, while gyroscopic forces prevail at $f > \omega$ (LeBlond & Mysak 1978). A notable location for diurnal tide trapping is the Kashevarov Bank (depth about 100 m). While the K_1 amplitude above this bank increases by only about 10 cm (see Fig. 6), the current at the top of the bank reaches 85 cm s^{-1}, while off-bank values are 5–10 cm s^{-1}. The maximum current of K_1 and O_1 is close to 160 cm s^{-1} at the bank's top.

Puerto Rio Gallegos, southern Argentina (Lat. 51°36′S Long. 69°01′W). Tidal range close to 12 m. The general chart of the M_2 tide (Fig. 1) shows strong amplification of this wave along the southern Argentinian coast. Such amplification is probably due to the wide shelf (Glorioso & Flather 1997). The width of this shelf is close to a quarter of the M_2 tide wavelength and resonant conditions may therefore be at work in this system. In Fig. 7 the amplitude and phase of the major diurnal (K_1) and semidiurnal (M_2) constituents are given on the basis of computations by Palma et al. (in press). They were kindly supplied by E. Palma, Universidad Nacional del Sur, Bahía Blanca, Argentina. The amplitudes of the diurnal waves are one order of magnitude smaller than the amplitude of the semidiurnal waves. The semidiurnal wave propagates from south to north and the largest amplitude of more than 4 m occurs along the shore between 48°S and 54°S in the Bahía Grande. Smaller bays to the north also enhance semidiurnal tides, and especially around 41°S (Golfo San Matias) the M_2 wave is strongly amplified so that the total tide range is close to 10 m. The largest tides occur in the estuary of Rio Gallegos. Measurements taken at Lat. 51°37′S, Long. 68°13′W during December 1980 (see Fig. 8) by the Departamento Oceanografia, Servicio de

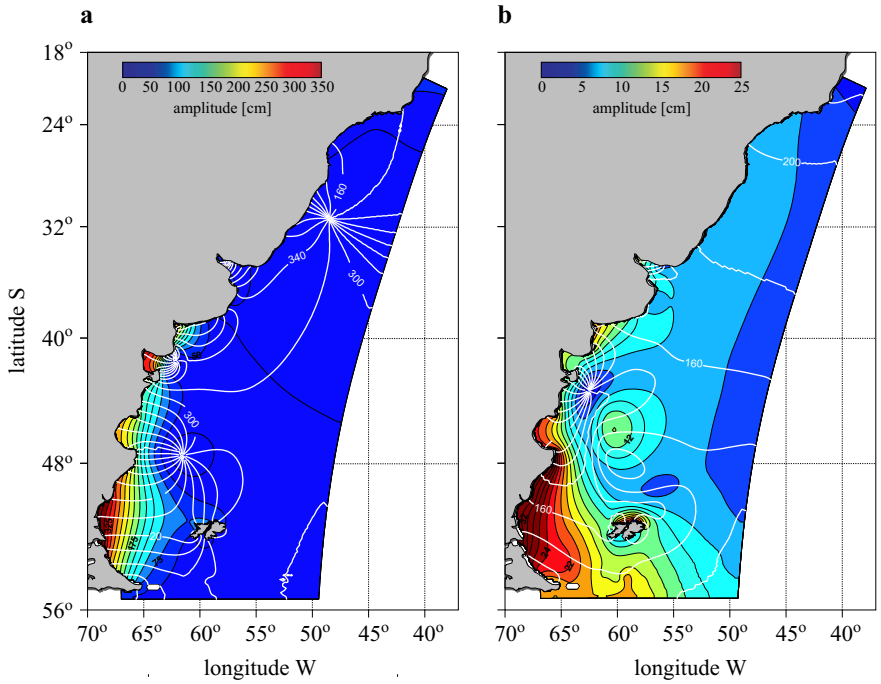

Fig. 7. Main tidal constituents: (a) M_2 constituent, amplitudes (color), Contour Interval (Cl) = 25 cm, Greenwich phase (white solid lines), Cl = 20 deg; (b) K_1 constituent, amplitudes (color), Cl = 2 cm. Courtesy of E. Palma, Universidad Nacional del Sur, Bahía Blanca, Argentina

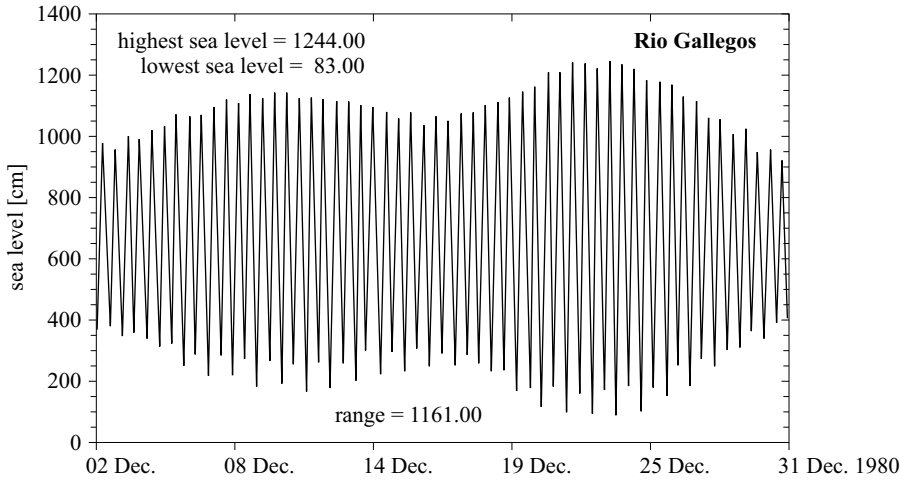

Fig. 8. Tide gauge records from Muelle El Turbio (Rio Gallegos) Lat. 51°37′S, Long. 68°13′W. Courtesy of the Departamento Oceanografia, Servicio de Hidrografia Naval, Argentina

Hidrografia Naval, show a range of 11.6 m, but up river from this point the range exceeds 13 m. Fig. 8 shows that the dominant tidal constituent is indeed a semidiurnal tide, but it also depicts a strong change in amplitude in the two-week period, which suggests that the tidal energy is highly variable in time.

Gulf of St. Malo, coast of France. At the port of Granville the maximum range of the spring tide reaches 14.7 m.

Bristol Channel, coast of England. The maximum tidal range in the Severn River estuary reaches 14.5 m.

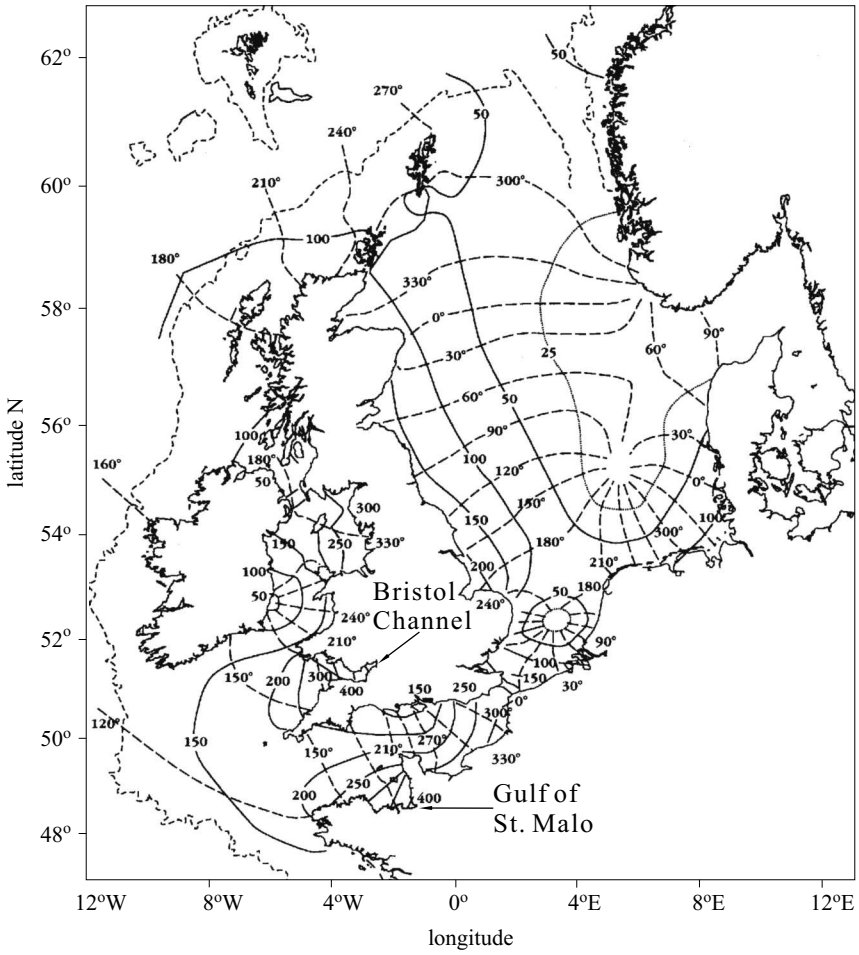

Fig. 9. Amplitude and phase of the M_2 tide in the north-west European Shelf Seas, based on Flather (1976). The amplitude (solid lines) is in cm and the phase (dashed lines, degree) is referred to Greenwich

The M_2 tide off the coasts of Scotland, England and France is strongly amplified as shown in Fig. 9. These data were derived by Flather (1976) through an application of the 2-D model. Computed amplitudes and phases are in close agreement with observations. In this figure, the two locations of the extreme tidal amplitude have been marked, the heads of the Gulf of St. Malo and the Bristol Channel. The English Channel/La Manche (between France and England) and Irish Sea (between England and Ireland) are two channels where the M_2 wave is generated through the interaction of two traveling waves entering these channels from the south and north (Defant 1960).

As both channels narrow, the tide is amplified, and it seems that, both in the Gulf of St. Malo, located in the English Channel/La Manche, and the Bristol Channel located in the Irish Sea, the resonance phenomenon is at work. The resonance interaction between the co-oscillating water-masses of the Gulf of St. Malo and the oscillations in the English Channel can

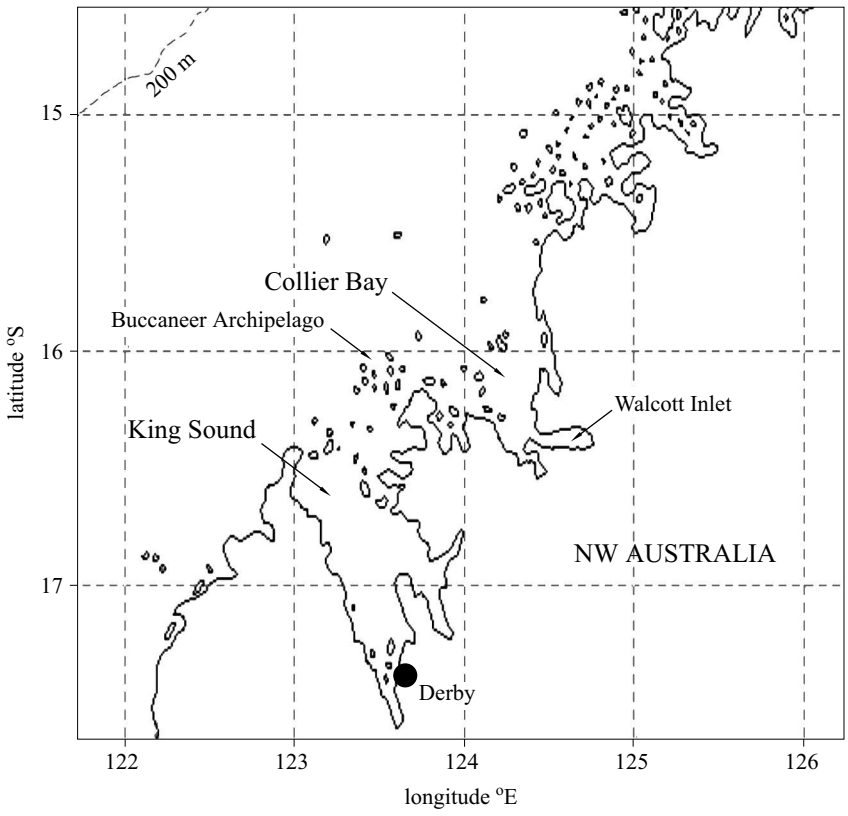

Fig. 10. North-west Australia. Geographical locations of the largest tides in the Australia. Notice the extent of the shelf given by the 200 m isobath

easily be deduced from Fig. 9. At the entrance to the Gulf of St. Malo the amplitude is only about 200 cm to 250 cm, while it increases to more than 400 cm at the head of the Bay. A similar situation occurs in the Bristol Channel; the amplitudes at the entrance of about 200 cm are amplified at the head of the Bay to approximately 450 cm.

North-west Australia. Tidal range 11 m. As can be gleaned from Figs 1 and 2, North-west Australia has very large tides. The major tidal constituents are semidiurnal tides. As in many of the cases considered earlier, the tidal behavior over an adjacent ocean shelf defines to a large degree the tides along the coastline. The largest tides occur in the two semi-enclosed water bodies: Collier Bay and King Sound (Fig. 10).

The largest recorded ranges in Australia are those for Lizard Island (11.352 m) and Shale Island (11.556 m) located in Collier Bay (see Fig. 11). This is based on data obtained in 1977 and 1963, respectively (NTF 2000). A common misconception is that the highest tides are around Derby, King Sound (10.468 m). The tides in King Sound and Collier Bay travel through narrow passages. The narrow passage to Talbot Bay (in the Buccaneer Islands) gives rise to very strong tidal currents. Tidal flow generates

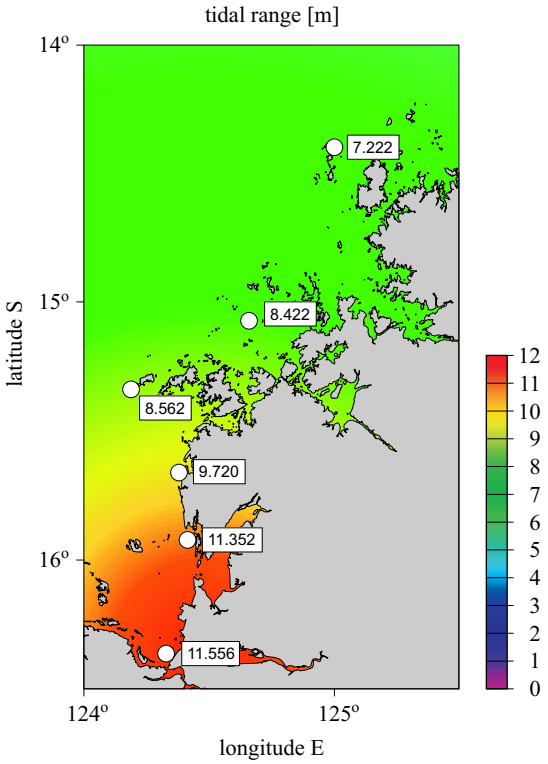

Fig. 11. Collier Bay, North-west Australia. Tide range in meters. Courtesy of the NTF, Australia

a waterfall effect as water piles up against one side of this narrow passage (50 m wide).

4. Rudimentary notions related to energy transfer

A force F applied to a water particle displaces this particle from position l to position $l + dl$, and therefore this force does the small amount of work dW

$$dW = Fdl. \tag{1}$$

The work done on the particle of water by the various forces is equal to the change in the kinetic energy of the particle. To understand this important connection between work and energy let us start with the general equation of motion,

$$\rho\frac{Du}{Dt} = F_x, \tag{2}$$

$$\rho\frac{Dv}{Dt} = F_y. \tag{3}$$

Here ρ denotes the density of the sea water, u and v are the components of the velocity vector along the x (East–West) and y (South–North) directions, respectively, and F_x and F_y are the components of force. Multiplying the first equation by dx and the second equation by dy, the work in the x and y directions is obtained:

$$\rho\frac{Du}{Dt}dx = \rho\frac{Du}{Dx}\frac{Dx}{Dt}dx = \rho\frac{Du}{Dx}udx = F_x dx = dW_x, \tag{4}$$

$$\rho\frac{Dv}{Dt}dy = \rho\frac{Dv}{Dy}\frac{Dy}{Dt}dy = \rho\frac{Dv}{Dy}vdy = F_y dy = dW_y. \tag{5}$$

Adding the above equations by sides

$$\rho d(u^2/2 + v^2/2) = dW_x + dW_y = dW \tag{6}$$

and integrating, we arrive at the conclusion that the work done by all forces in the system, such as pressure, tidal forces and friction result in a change in the kinetic energy of the system.

$$\rho(u^2/2 + v^2/2)_2 - \rho(u^2/2 + v^2/2)_1 = W. \tag{7}$$

To continue this consideration, one needs a system of units to measure forces, work and energy. The force defined by eqs. (2) and (3) is density

multiplied by acceleration. This is due to the fact that we are considering the mass of unit volume. Thus, assuming force to be mass times acceleration,

$$F = m\frac{Du}{Dt}; \quad \text{units in CGS are} \quad 1 \text{ g} \times 1\frac{\text{cm}}{\text{s}^2}. \tag{8}$$

This unit is called a dyne. Since 1 kg=10^3 g and 1 m s^{-2} = 10^2 cm s^{-2}, a larger unit, called a newton, is introduced. 1 N=1 kg$\times$ 1m s^{-2} = 10^5 dyne. The unit of work is defined as the work done by a unit force moving a water particle a unit distance. In CGS the unit of work is 1 dyne $\times$ cm, which is called an erg. Finally, the notion of power is defined as the time rate at which work is done,

$$P = \frac{dW}{dt} = Fu; \quad \text{units in CGS are} \quad 1 \text{ J/s} = 10^7 \text{ erg} = 10^7 \text{ g} \times \frac{\text{cm}^2}{\text{s}^3}. \tag{9}$$

From the above, the power can also be expressed as force multiplied by velocity. 1 J s^{-1} is called a watt (W).

It is of interest to evaluate the amount of tidal energy which can be used for tidal power. Here different avenues can be taken; the easiest approach is to define potential energy, as it is expressed by sea level change; the average numbers for this change are easily accessible from measurements. The kinetic energy is expressed by currents and is therefore a less well-known part of the energy balance. Besides kinetic and potential energy, the consideration of energy dissipated due to friction may also be important, because redirecting this energy into tidal power seems to sustain the tidal regime. The average dissipated power due to tides is equal to 4 TW (Munk 1997, Egbert & Ray 2000) and the major portion of approximately 3 TW is associated with the lunar tides (Kagan 1997), (1 Terawatt = 10^{12} W). Generally, we assume that the work done by the Moon and Sun is in balance with the tidal energy dissipated in the World Ocean. The efforts of oceanographers to evaluate the energy dissipated through the work done by the frictional forces and through other tidal energy sinks are still in progress (Munk 1997). The exploitation of tidal energy should reinvest this dissipated energy into tidal power on the tacit assumption that such an approach should not seriously disturb the tidal regime. The substantial changes introduced by tidal power tapping may defeat the entire purpose of tidal power. The present-day tidal current and tidal elevation may remain unchanged if tidal dissipation is substituted for tidal energy tapping. While the amount of dissipated energy is relatively easy to account for, the spatial (geographic) distribution of dissipation will be difficult to preserve (or restrict to the natural dissipation), since tidal energy must be tapped

strongly in a smaller domain to be economically viable. To estimate the available tidal energy, the kinetic and potential energy of the tides neeeds to be known. The potential energy is given by

$$\frac{1}{2}\int\int \rho g\zeta^2 dxdy = \text{const.} \tag{10}$$

This energy is expressed in $\mathrm{g}\times\mathrm{cm}^2\ \mathrm{s}^{-2}$; therefore to change it into power it has to be divided by time, i.e. the tidal period. Here ζ is the sea level, which changes from 0 to the tidal range, or $2\zeta_a$ during the tidal period, where ζ_a is the amplitude. The major input into this expression is the surface area of a domain. Let us estimate the potential energy in Cook Inlet, Alaska, where the maximum tidal range is close to 11 m and the average range over the inlet can be taken as 6 m. The surface area of the inlet is approximately 2×10^4 km^2. Substituting these numbers in the equation for the potential energy, we arrive at 3.5×10^{15} J$= 3.5 \times 10^3$ TJ. Assuming that this energy can be changed into power at a constant rate in time during the M_2 tide period, the power extracted will be 7.8×10^{10} W $= 7.8 \times 10^7$ kW. Similar calculations for the entire World Ocean with an average tide amplitude of 50 cm will yield a global energy equal to 3.5×10^5 TJ. Changing this energy into power, we arrive at approximately 8×10^9 kW. This power is only 100 times larger than the power available in Cook Inlet, although the surface of the World Ocean (5×10^8 km^2) is about 2.5×10^4 times larger than that of Cook Inlet. Finally, a word of caution: formula (10) used for the potential energy calculations gives only an approximate estimate. The formula is right, but it requires detailed knowledge of sea level distributions.

Actually, the energy calculated above cannot be extracted into power uniformly in time. The tide is variable in time, and in Cook Inlet it exhibits a marked diurnal inequality with consecutive high and low waters varying strongly. The tidal regimes in all local waters display strong fortnightly (neap-spring) variability, see, Fig. 8. Usually the amplitudes from spring to neap tides change by a factor of 2, which means that energy changes by a factor of 4. These variabilities make the utilization of tidal energy quite difficult and necessitates large investments in complicated machinery for power generation, which differs from hydro-power generation. However, we have to realize that 'available' tidal energy cannot be completely used for power generation; the best approach will be to utilize the portion which is dissipated in the local water body. This guarantees (to some degree) that the old tidal regime will remain undisturbed. A different approach is to use tidal energy only in a small section of the basin (bay), so that even if the tidal regime is changed the remaining area of the basin will sustain strong tides and deliver energy for power tapping.

5. Tidal energy balance in local water bodies

The energy balance equation averaged over the tidal period includes energy sources, i.e. energy generation due to the work of external forces, as well as energy sinks, that is, the energy dissipated by internal and bottom friction. Sources and sinks of energy are connected by the transport of energy expressed by the energy flux (Munk 1997). The well established principle of energy conservation states that the tidal energy averaged over the tidal period and over the surface of the local water body must remain constant; therefore, the tidal energy flux into a local domain (across open boundaries) and the tidal energy generated in this domain ought to be in equilibrium with the dissipation. Hence, for the energy balance over the tidal period and over the domain surface and boundaries, a simple equation holds (Nekrasov 1990, Kowalik & Murty 1993, LeProvost & Lyard 1997):

$$\frac{1}{T}\int\left\{\int\int\left[E_g+\frac{\partial E_{hx}}{\partial x}+\frac{\partial E_{hy}}{\partial y}=E_d\right]dxdy\right\}dt, \tag{11}$$

where $dxdy$ is an element of the surface in the x and y coordinates, t is time, T denotes the tidal period, and $E_g = E_{gx} + E_{gy}$ is the surface density of the energy generated in the domain expressed in W cm^{-2}. Therefore, to derive the total energy, this is multiplied by the domain surface area. E_{hx} and E_{hy} are components of the energy flux across the boundary between the local water body and the ocean, expressed in W cm^{-1}. To derive the total inflowing energy it is multiplied by the length of the boundary. E_d is the surface density of the energy dissipated in the domain and is expressed in W cm^{-2}. Hence, to derive the total dissipated energy, it should be multiplied by the surface area of the domain. Usually, the tidal energy generated in a local domain is very small in comparison to the energy flux, so that an even simpler equation of energy conservation can be written:

$$\frac{1}{T}\int\left\{\int\int\left[\frac{\partial E_{hx}}{\partial x}+\frac{\partial E_{hy}}{\partial y}=E_d\right]dxdy\right\}dt. \tag{11a}$$

The energy flux is a vector with two components defined as (Nekrasov 1992, Henry & Foreman 2001),

$$\mathbf{E}_h = \{\rho g H u\zeta,\ \rho g H v\zeta\}. \tag{12}$$

Here the following notation is used: ρ is the density of water, g is the acceleration due to the earth's gravity, H is the water depth, ζ is sea level, and u and v are velocity components in the west–east x and south–north

y directions. Investigation of the progressive tidal wave established the mean energy flux (over the tidal cycle) in the x direction as

$$\bar{E}_{hx} = \frac{1}{2}\rho g H u_a \zeta_a \cos(\phi_u - \phi). \tag{13}$$

A similar formula can be written for the y coordinate

$$\bar{E}_{hy} = \frac{1}{2}\rho g H v_a \zeta_a \cos(\phi_v - \phi). \tag{14}$$

The measured sea level and velocity are represented here as the cosine of the frequency $\omega = 2\pi/T$ (T is the tidal period), and time t. The sea level and velocity in the tidal wave are given in the following way:

$$\begin{aligned} \zeta &= \zeta_a \cos(\omega t - \phi), \\ u &= u_a \cos(\omega t - \phi_u), \\ v &= v_a \cos(\omega t - \phi_v), \end{aligned} \tag{15}$$

where ζ_a is the amplitude and ϕ is the phase of a tidal wave. For each tidal constituent the amplitude and phase are called harmonic constants. u_a and ϕ_u are the amplitude and phase for the u component of the current (u harmonic constants), v_a and ϕ_v are the amplitude and phase of the v component of the current (v harmonic constant).

Tidal energy dissipation takes place through bottom friction, horizontal friction and transfer of tidal energy into internal tides or turbulence (cf. Munk 1997). The most important terms are due to dissipation by bottom friction:

$$E_{dx} = \rho u \tau_x^b \qquad \text{and} \qquad E_{dy} = \rho v \tau_y^b. \tag{16}$$

Here τ_x^b and τ_y^b are components of the bottom stress, which depends on the current velocity and is expressed as

$$\tau_x^b = \rho c_d u \sqrt{u^2 + v^2} \quad \text{and} \quad \tau_y^b = \rho c_d v \sqrt{u^2 + v^2}. \tag{17}$$

The dimensionless bottom drag coefficient c_d is approximately equal to 3×10^{-3}. The total dissipated energy

$$E_d = E_{dx} + E_{dy} = \rho c_d u^2 \sqrt{u^2 + v^2} + \rho c_d v^2 \sqrt{u^2 + v^2} = \rho c_d (u^2 + v^2)^{3/2} \tag{19}$$

is proportional to the velocity cubed.

According to eq. (11), the above term is first averaged over the tidal period and subsequently integrated over the surface of the entire domain. The rate of energy dissipation is expressed in erg s^{-1} cm^{-2}, while the net energy flux across a transect is expressed in erg s^{-1} cm^{-1}. We are going to demonstrate the distribution of energy in the Sea of Okhotsk for the K_1 wave. The energy flux for the K_1 constituent, calculated by Kowalik & Polyakov (1998), is shown in Fig. 12. The energy flux across the open eastern boundary brings 100.5×10^{16} erg s^{-1} into the computational domain (this domain also includes a portion of the Pacific), while the flux of 27.8×10^{16} erg s^{-1} through the southern boundary is directed into the Pacific from the Sea of Okhotsk.

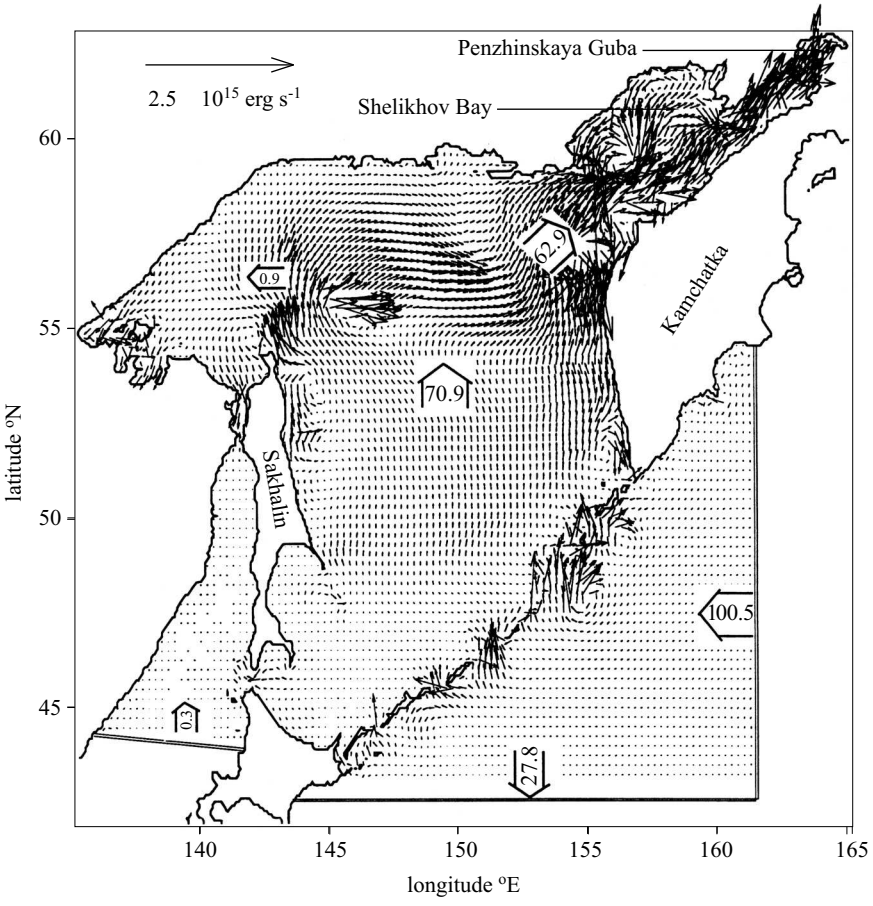

Fig. 12. Tidal energy flux for K_1 tide in the Sea of Okhotsk based on Kowalik & Polyakov (1998). The large arrows show the net energy flux across transects. The values inside the arrows should be multiplied by 10^{16} erg s^{-1}

Additionally, a very small flux of 0.3×10^{16} erg s^{-1} is directed from the Sea of Japan into the Sea of Okhotsk domain. The net flux of tidal energy is directed from the open boundary located in the Pacific Ocean through the Kuril Straits towards the region of high frictional dissipation in Shelikhov Bay and Penzhinskaya Guba. The large open arrows in Fig. 12 show the net energy fluxes (energy flux multiplied by the length of a transect) crossing several transects. The general pattern of energy flow is broken by the larger and smaller domains of a circular or semicircular flux of energy. These are regions of trapped tidal energy and enhanced flux. The areas around the Kuril Islands (especially on the Pacific side), the Kashevarov Bank and the entrance to Shelikhov Bay are major domains of trapped energy. Lesser domains are located at the escarpments between the Kashevarov Bank and the entrance to Shelikhov Bay, along Kamchatka and Sakhalin.

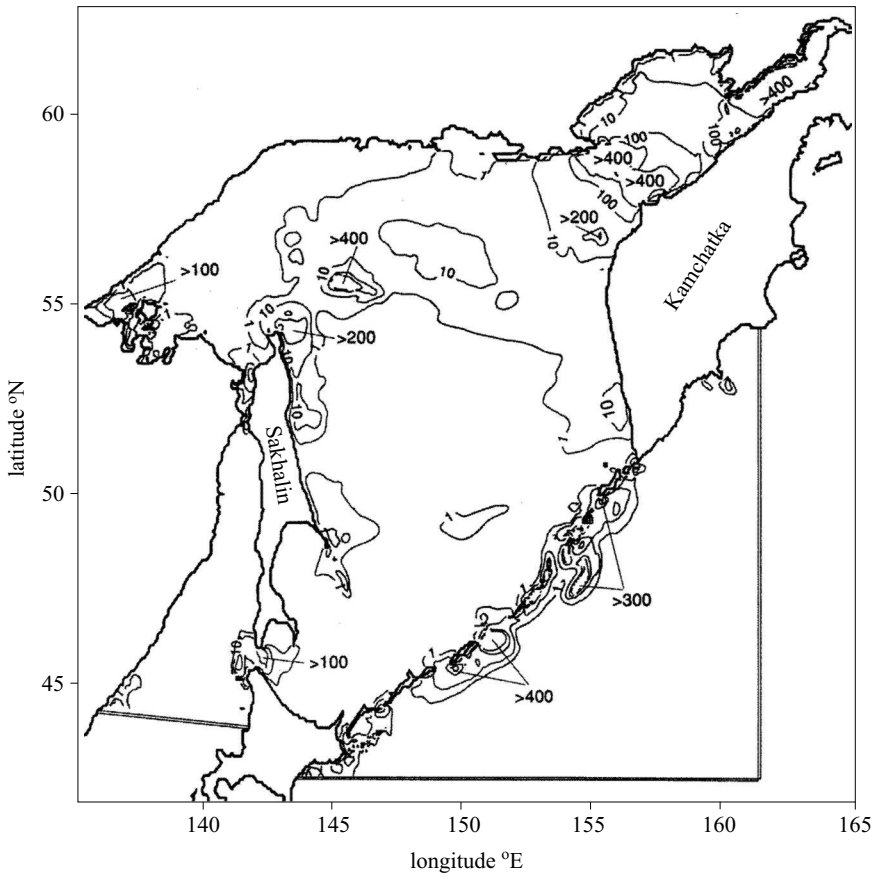

Fig. 13. The rate of energy dissipation per unit surface due to K_1 tide (erg s^{-1} cm^{-2}) in the Sea of Okhotsk based on Kowalik & Polyakov (1998)

Fig. 13 depicts the rate of energy dissipation per unit surface in the Sea of Okhotsk due to the K_1 constituent. The trapping of the energy flux over the local bathymetry depicted in Fig. 12 for the K_1 constituent resulted in local maxima for the rate of energy dissipation. The overall rate of energy dissipation of the K_1 wave due to bottom friction is obtained by integrating over the surface of the entire domain given in Fig. 13. In Table 1 the total energy balance is shown for the four tidal constituents K_1, O_1, M_2 and S_2. For the major constituent K_1 the total energy source, i.e. inflow and generation by astronomical forcing, is equal to 77.7×10^9 W, and is close to the energy sink caused by bottom and horizontal friction dissipation.

Table 1. Energy balance for the major tidal constituents

Net flux through open boundary:	Sources $\times 10^9$ W				Rate of energy dissipation due to:	Sinks $\times 10^9$ W			
	K_1	O_1	M_2	S_2		K_1	O_1	M_2	S_2
Sea of Japan	0.3	0.3	−0.05	0.0	bottom friction	58.1	17.5	39.9	3.4
Southern boundary	−27.8	−11.4	−15.8	−1.3	horizontal friction	20.2	7.8	9.3	1.1
Eastern boundary	100.5	34.4	56.3	5.4					
Energy generation by astronomical force	4.7	1.3	8.1	0.5					
Total	77.7	24.6	48.6	4.6		78.2	25.2	49.2	4.5

The total energy flux across open boundaries and the overall rate of energy generation due to astronomical tidal forcing is balanced by the total rate of energy dissipation. The net energy flux across the open boundaries is the principal source of energy. The overall rate of energy generated by astronomical forces is relatively small. For the the K_1 tide, astronomical forces generate only 4.7×10^9 W, approximately 6% of the total energy. The total rate of energy dissipation due to the K_1 tide dominates the dissipation due to the M_2 tide, since the overall rate of energy dissipation due to the M_2 wave is only 49.2×10^9 W.

6. Tidal power from bays of high tidal energy

Consider a bay with a large tidal range (Fig. 14) connected through a relatively narrow entrance to the open ocean. Here we would like to investigate various methods of tapping the tidal energy and the possible consequences of a closure placed across the entrance to the bay. Generally, a structure placed across the entrance may be directed either to tapping potential energy and utilizing the power through the difference in sea level

generated by the dam, or a number of generators can be placed to tap kinetic energy. Computations related to tidal power extraction need to estimate the effects of a structure placed across the entrance on the tides in the bay. Usually, bays with large tides, like Cook Inlet in the Gulf of Alaska, the Bay of Fundy on the Atlantic coast of North America or the White Sea in Northern Russia cause amplification of the tide from the mouth to the head of the bay. Such tidal patterns may be attributed either to the gradual shallowing and narrowing of bays or resonance conditions, when the bay's own period of oscillations is close to that of the tidal period. Any structure in the upper reaches of such a bay may result in a change in the tidal pattern which tunes the bay either closer to resonance, in which case larger tidal ranges are the result, or away from resonance, causing smaller tidal ranges (Garrett 1984). For the Bay of Fundy the estimate is that the bay is a little too long for full resonance; similarly, the estimates for Cook Inlet suggest that it is also rather too long for resonance. Blocking off part of the bays may bring about a different tidal regime: in both the Bay of Fundy and Cook Inlet a higher tide range will occur, since further shortening of the bays may tune them closer to full resonance. The complete blocking of the upper end of Minas Basin in the Bay of Fundy (see Fig. 5) performed in a numerical model by Greenberg (1979) does not generate such a clear picture as one would expect from the simple resonance consideration: the sea level dropped close to the barrier, but increased in the rest of the Bay of Fundy. To offset such a reduction in tidal range, a larger number of generating units is usually installed at a tidal power station. This, in turn, will lead to further sea level reduction due to partial blocking of the flow by the turbines.

The environmental changes induced by a dam or barrage also lead to changing patterns of tidal currents. Cook Inlet is known for its large and variable deposits of sediments, as tidal currents often are in the range of several knots. A barrage may give rise to stronger currents, leading to the complete scouring of sediments in some locations and their redeposition in other locations. It is important to use sediment transport models that will simulate the influence of the structure on the net sediment transport: the shipping channels cannot become areas of deposit and the sand cannot be removed from the beaches. The study of the sedimentation patterns in the Bay of Fundy and Minas Basin by Pelletier & McMullen (1972) showed that sedimentary regime in Minas Basin is in equilibrium. If the tidal regime were to be changed by a dam, the delicate equilibrium would be destroyed, leading to large deposits in some locations. Therefore, in choosing a construction site and a method of extracting tidal power, a balance must be achieved between the cost of construction, environmental changes and the quantity

of generated energy. The latter is quite easy to evaluate, based on the simple computation we have made above. The environmental consequences can be deduced with the help of numerical models (see Kantha & Clayson 2000).

Since placing a dam or turbines in the tidal flow will introduce a resistance into this flow, we can assume that the current and sea level will become smaller farther from the structure. Close to dams, currents are very strong and the turbines create a lot of turbulence. Potentially, large numbers of fish may pass through the turbines, which will sustain considerable damage as a result. In regions of strong currents, methods ought to be defined for impact predictions on fish and marine life, and measures should be implemented to avoid areas of strong currents and turbulence. On other hand, the slower currents farther away from a dam will influence the flushing rate of the bay, which in turn may influence the rate of pollution.

Water temperatures in the bay may change as well; this often happens because of mechanical mixing. Sluggish currents in the bay will reduce mixing, which in turn may result in more extreme seasonal temperatures. Thus, the consequences of tidal power structures are many and often difficult to predict. The basic prediction may be supported by the equations of motion and continuity described in Kowalik & Murty (1993). The three subdomains shown in Fig. 14 are components of a hydrodynamical-numerical model for predicting elevations and currents. All subdomains should be connected by the boundary conditions. Starting from the open ocean, the time-variations of sea level at the open boundary can be described from observations or larger scale models (in Fig. 14 it is given as $\zeta_0 \cos(\omega t)$). Next, by means of numerical solutions, the sea level and velocity can be

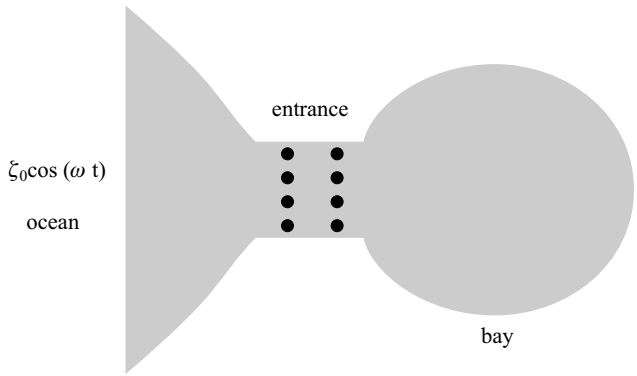

Fig. 14. Diagram of a TPP and hydrodynamical modeling in a bay with a large tidal range. In the ocean the tide is described by $\zeta_0 \cos(\omega t)$, the dots represent a tidal barrage or tidal current generators

calculated in the entrance to the bay. Before this calculation can be tackled, however, the flow rate through a dam, barrage or turbines must be given. The flow through turbines ought to be connected with the inner subdomain represented by the bay. Such an approach will allow currents and sea level distribution to be calculated, before and after a structure is placed across the entrance to the bay. More sophisticated equations taking sediment motion and heat transport into account will provide answers to the more complicated environmental questions.

7. Tidal power from sea level differences

The generation of power from tides is not very different from hydropower generation using river flow. The main requirement is a difference in water level to drive the turbines. There are many schemes for tidal power generation; the simplest one is presented in Fig. 15. A single basin (bay) is cut off from the open ocean by barrages. The barrage incorporates sluice gates and a power station housing the turbines. The barrages create the water head necessary for turbine operation. The sluices control the water flow for power generation, navigation and sometimes for fish migration. In the so-called one-way (single-effect) generation, the incoming tide enters the bay through the sluice gates and turbines and on the ebb tide the water exits through the turbines. To keep the maximum level inside the bay the sluice gates are locked and power generation is achieved during the ebb tide (Gibrat 1966, Bernshtein 1996).

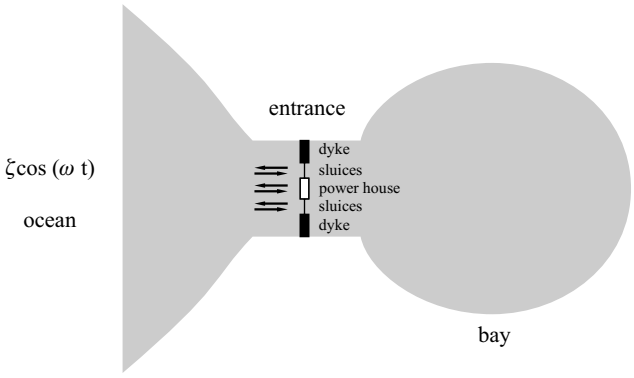

Fig. 15. Tidal power plant constructed at the entrance to a single bay

To start power generation, a minimum sea level difference (minimum head) between the ocean tides and basin tides is required (Fig. 16). To generate the minimum economic head for power production a tidal range of

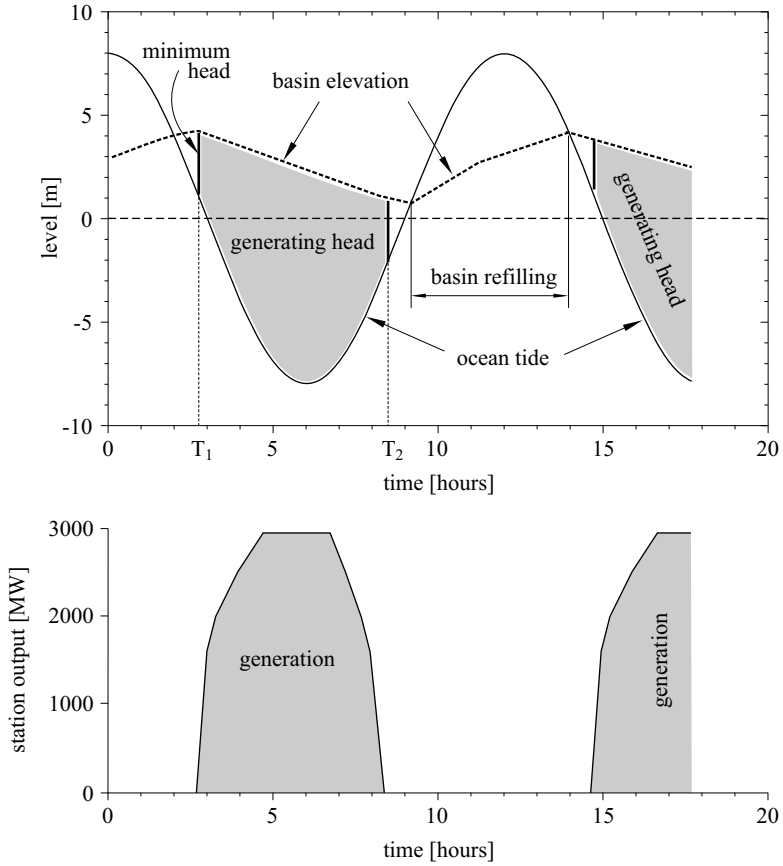

Fig. 16. Tidal power generation: typical one-way cycle for a single bay. Upper panel, sea level inside and outside the bay. Lower panel, power output in time

4 to 6 m is needed. Typical sea level variations outside and inside the basin are shown in Fig. 16, upper panel, for a semidiurnal tide. The presence of sluices and turbines limits the flow of water between the bay and the ocean. This reduces the range of sea level change inside the bay as compared to the sea level before TPP construction. The time span when sufficient sea level differences exist for power generation is limited by the minimum head required. The power generation time is also limited by the time needed for the basin to be filled on the rising tide. For the minimum head assumed in Fig. 16, the generation time (from T_1 to T_2) is approximately 5.5 hours. As can be seen in the lower panel of Fig. 16, the generators do not deliver constant power in time during each generation cycle. The power output increases slowly with the increasing head up to a level when constant power is achieved. Often, due to the high available head the turbine output needs to be cut back to avoid overloading.

The general picture from the above scheme is that the available power is highly variable in time, which points toward development of various schemes of economical and controllable utilizations of tidal power.

Such schemes have been achieved mainly through the investigations of French scientists and engineers and implemented in the 240 MW TPP at La Rance, Brittany, France, constructed in 1967 (Gibrat 1966). About 750 m wide, the La Rance estuary was an ideal site with its 18 000 m^3 s^{-1} flow at the flood tide. The estuary (behind the dam in Fig. 17) is capable of containing about 180 million m^3 of water in a basin area of 22 km^2. The estuary was blocked by a 13 m high dam. This dam (Fig. 17) also serves as a highway bridge between St. Malo and Dinard. The power station operates in a one-way mode, illustrated in Fig. 17, although two-way operation (on both the ebb and flood tides) is possible. In two-way operation the rotation of the turbine in Fig. 17 can be reversed to follow the ebb/flood cycle. 240 MW is probably the maximum output (not sustainable all the time); nevertheless, even if an average is only 50% of the maximum, La Rance delivers 120×10^3 kW $\times$ 8760 h $= 1.05 \times 10^9$ kWh per year. To estimate the number of homes that this quantity of electricity can be supplied to in a year, the average household consumption is assumed to be about 4500 kWh $year^{-1}$. Thus the La Rance tidal power station supplies about 222 thousand households.

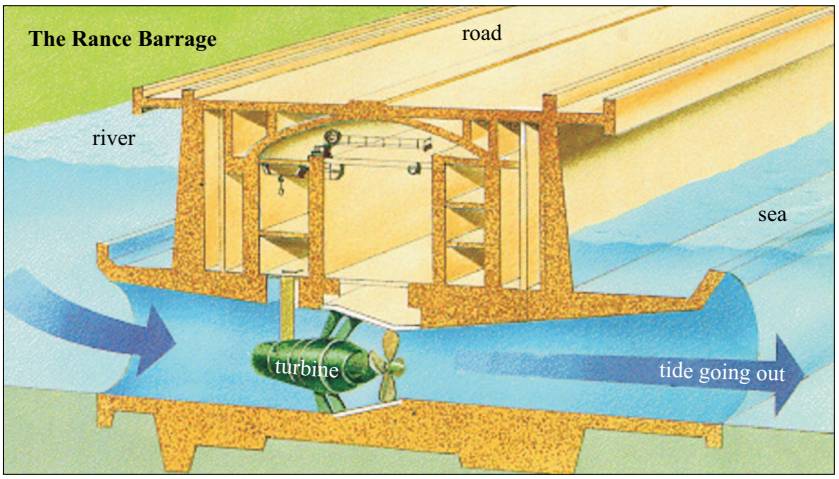

Fig. 17. La Rance tidal power station. Courtesy Electricité de France

The Russian and French investigations served well in developing a TPP at the Kislaya Guba in the Barents Sea on the Kola Peninsula, Russia in 1968, with an installed power of 0.4 MW and a small artificial basin of area 1.1 km^2. An 18 MW plant was built in 1984, at Annapolis Royal (entrance

to the Annapolis river in the Bay of Fundy), Nova Scotia, Canada. The area of the basin behind the barrage is only 15 km^2. In 1985, China constructed a small plant at Jiangxia with a 4 MW output and a small basin area of 1.4 km^2. New tidal power plants are being considered, including the Severn project in England and in Garolim Bay, Korea.

A more efficient use of sea level difference is to generate power on both the rising and falling tides (Gibrat 1966, Bernshtein 1996). This is called 'single-basin two-way generation'. Previously, the power was generated on the falling (ebb) tide only when the minimum head required for power generation occurred at time T_1 and lasted untill time T_2 (cf. Fig. 16). In the new regime, at time T_2 the turbines are stopped, rotated in the opposite direction and restarted at time T_3, when the minimum sea level difference on the rising (flood) tide occurs.

This regime lasts until time T_4, when the turbines are stopped and reversed. From Fig. 18 it can be deduced that a TPP working in the two-way regime delivers power during 8.5 h, compared to the one-way generation time of 5.5 h.

The efficiency of the TPP can be improved in many ways: the use of pumping is a very common method for raising the sea level inside the basin and therefore gives a better power output. In connection with the utilization of tidal power in the Bay of Fundy (Fig. 5), many utilization schemes have been suggested because of the proximity of two bays (Chignecto and Minas Bays) with high tides. The paired-basin schemes provide the opportunity for continuous power generation (Lawton 1972).

A simple theory for designing a TPP has been described by Gibrat (1966), Prandle (1984) and Godin (1988). This theory links generated power to the sea level changes in the basin and discharge through the dam. The water level inside the basin is denoted as $Z(t)$ and the sea level in the ocean as $\zeta = \zeta_0 \cos \omega t$. The sea level difference or head H_d is given by

$$H_d(t) = Z(t) - \zeta_0 \cos \omega t. \tag{19}$$

Denoting discharge through the turbines during the power generation phase as Q and assuming it is constant in time, we can write the continuity equation in the following form,

$$S \frac{\partial Z}{\partial t} = -Q. \tag{20}$$

Here, S is the surface area of the basin, $\frac{\partial Z}{\partial t}$ is the vertical velocity of the free surface. The positive direction of discharge is from the basin to the ocean. An additional assumption is that the surface area of the basin,

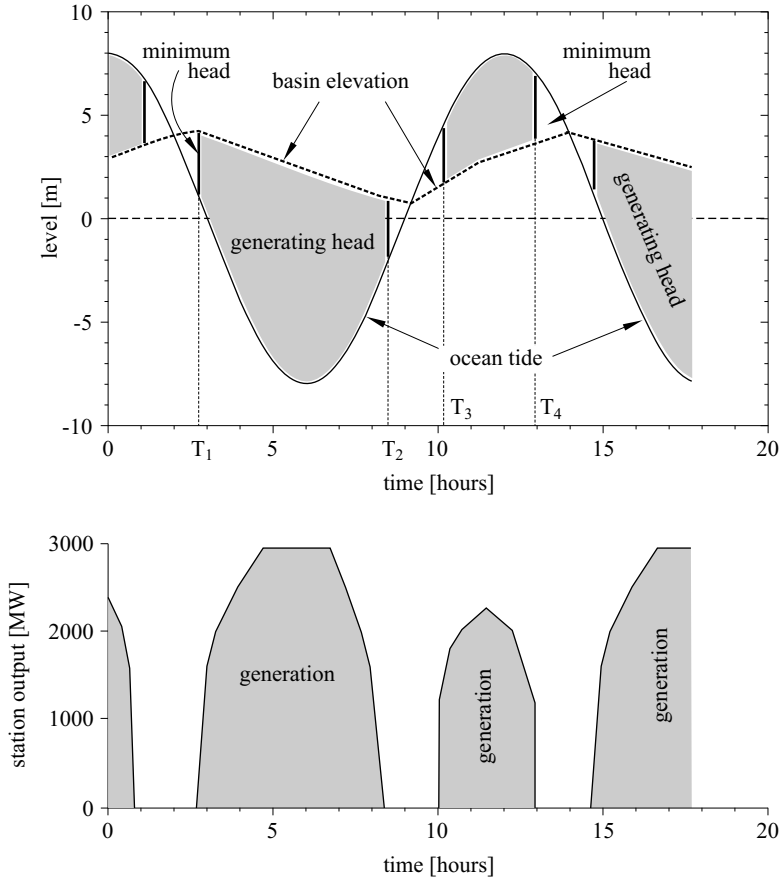

Fig. 18. A typical two-way cycle for a single bay. Upper panel, sea level inside and outside the bay. Lower panel, power output in time

though moving up or down, does not change in time. Neglecting losses, the principal parameter for the tidal plant evaluation, the power produced (PW), is given by

$$PW = \rho g H_d Q. \tag{21}$$

Therefore, the energy extracted during one tidal period (see Fig. 16) is

$$E = \rho g \int_{T_1}^{T_2} H_d Q dt. \tag{22}$$

Introducing the definition for the head given by eq. (19) and assuming that the discharge is constant

$$E = \rho g Q \int_{T_1}^{T_2} H_d dt = \rho g \int_{T_1}^{T_2} (QZ(t) - Q\zeta_0 \cos\omega t) dt =$$

$$\rho g \int_{T_1}^{T_2} \left(QZ(t) - Q\zeta_0 \cos\omega t \right) dt = \rho g \int_{T_1}^{T_2} \left(-S\frac{\partial Z}{\partial t} Z(t) - Q\zeta_0 \cos\omega t \right) dt =$$

$$\rho g \left[-S \int_{Z_1}^{Z_2} Z dZ - Q\zeta_0 \int_{T_1}^{T_2} \cos\omega t \right] =$$

$$-\rho g S \left[\frac{Z_2^2 - Z_1^2}{2} - \left(\frac{Z_2 - Z_1}{T_2 - T_1} \right) \frac{\zeta_0}{\omega} (\sin\omega T_2 - \sin\omega T_1) \right], \tag{23}$$

where Z_1 and Z_2 are the sea level in the bay at times T_1 and T_2. Thus, the energy is extracted through the complicated interaction of the levels inside and outside the bay. When the question about the possibility of tapping tidal energy from a semi-enclosed bay was asked, we used the expression for the potential energy to evaluate this energy, see eq. (10). This expression obviously gave the maximum available energy. The total available energy is present in the above expression; this is the term related to $(Z_2^2 - Z_1^2)$. The portion of the total available energy fluxed back to the ocean is given by the last term in eq. (23). The relation of this term to the energy flux given by eq. (12) is easily established, since the discharge Q is actually the horizontal velocity integrated over the cross-section of a channel.

Eq. (23) defines the extracted energy during the ebbing cycle in Fig. 16. The basin refilling regime, when the sluice gates are open, is given by the following discharge

$$Q = \epsilon G \sqrt{2gH_d}, \tag{24}$$

where, G is the sluice gate area, and ϵ is a flow contraction coefficient depending on the shape of the structure. $G_\epsilon = \epsilon G$, where G_ϵ is the effective gate area. Introducing this discharge into eq. (20) and taking into account the equation for the head,

$$\frac{\partial Z}{\partial t} = -G_\epsilon \sqrt{2g(Z - \zeta_0 \cos\omega t)}. \tag{25}$$

From the above we can conclude that the effective sluice gate area is a function of the square root of the head during the sluicing time, while the power produced by the turbine is proportional to the head value. This exemplifies the difference between the sluicing and the generating phases of the process. The large tidal waves (large heads) increase the efficiency of tidal power generation. On the other hand, using a large basin with a large

surface area will increase the extracted energy, but it also increases the losses from sluice gate operation. The gates are required to open and close during each tidal cycle, which may amount to as many as 700 operations per year, while in a standard hydro-power station the gates will be open only a few times per year. With both gains and losses of energy being variable in time, optimization methods were applied to obtain the maximum energy yield from tidal power plants (see Gibrat 1966 and Bernshtein 1996).

8. Tidal power from currents

8.1. The future of tidal power

The older approach to power generation was to block the entrance to the bay with a dam and use the difference of the sea level in front and behind the dam to move the turbines. The cost of building dams and tidal generating stations is often prohibitive. The estimated cost of the proposed tidal station on the River Severn in England would be in the range of $15 billion. The recent approach is to place turbines (tidal flow generators), devices similar to wind-mills, into the tidal current. The construction, operating and maintenance costs of such tidal flow generators is much lower compared to barrages. Additionally, the environmental changes introduced by turbines are much smaller than the changes caused by damming the entire bay entrance. The propeller of the tidal flow generator is quite slow, with 4 to 6 rotations per minute. Since the power generated from the flow is a function of the fluid density, the propellers constructed for water do not need to be as large as for air. A new helical water turbine has been patented by Gorlov (2001). This turbine captures 35 percent of the water's energy (http://www.gcktechnology.com/GCK/pg2.html). A few tidal power plants already use tidal power from currents. A TPP with helical turbines has been tested in the Uldolmok Strait, Korea, where the speed of tidal currents reaches 6 m s^{-1}. The New York Power Authority and Columbia University are deploying a demonstration turbine system in the East River in New York City. This system will also be used for field testing and design prototyping. In tidal currents of up to 7.5 knots, a generator with 10-foot diameter blades will be capable of generating up to 25 kW (http://www.verdantpower.com/Initiatives/eastriver.shtml). In 2002, the Norwegian company Hammerfest Stroem deployed tidal flow generators in northern Norway close to the town of Hammerfest. The 300 kW turbines are located at the bottom of a narrow strait, well below the surface, so that shipping is unhindered. The blades of the propellers can be rotated to adjust for the tidal current direction (Stone Future 2003). TPP construction and

operation will depend on the existence of a large-current location in close proximity to local users.

Tidal power plants have the potential to provide large amounts of energy. The European Commission has estimated that 42 sites of large tidal currents around the UK could produce 48-terrawatt hours of electricity per year. The Commission has identified large tidal currents at 106 sites around Europe.

One of the most interesting tidal flow generators and one that is stimulating tidal power development is the Stingray, constructed by The Engineering Business Ltd. (EB, Northumberland, UK). Let us carefully analyze the many facets involved in constructing, testing and operating such generators. The kinetic energy of tides is converted into electricity by a hydraulic generator system. The key feature of this machine is a large horizontal hydrofoil which by means of pitch control (angle of attack) can oscillate up and down (Fig. 19). This motion forces a support arm to oscillate up and down as well. The arm is restrained by hydraulic cylinders, which produce high-pressure oil that drives a hydraulic motor and then hydraulic pressure rotates the generator. The generator output feeds an industrial drive system giving a dc output. In a Stingray farm, the output from a number of devices feed a dc bus which typically connects through a submarine cable to land, where an invertor produces ac power for users. The initial plan (Trapp & Watchorn 2001) was to develop a machine with a 150 kW time-averaged output in a 2 m s^{-1} current. Stingray had to

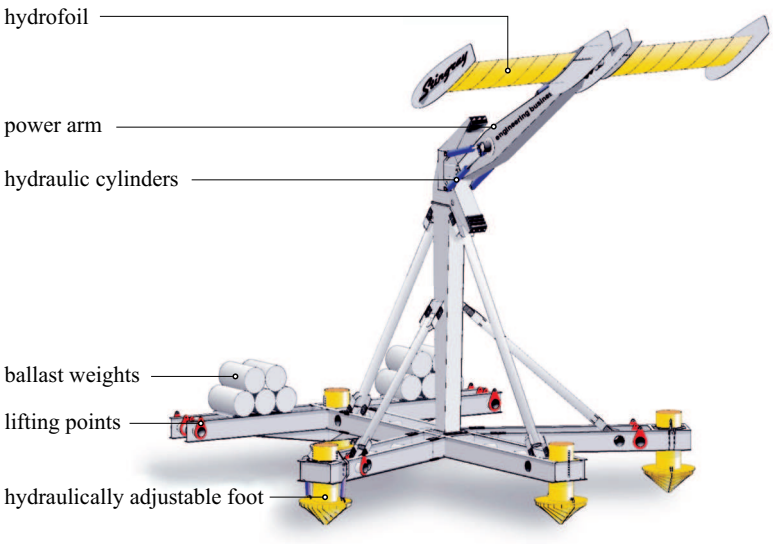

Fig. 19. Stingray tidal current generator. Courtesy, The Engineering Business Limited (http://www.engb.com)

be designed so that the whole assembly could be installed and recovered easily at low cost, and as often as required. Since hydroplane design and control was very important in achieving high power output from Stingray, EB carried out extensive dynamic modeling of the hydroplane and arm movement. The second stage was the preliminary testing of the machine, as well as the launch and recovery system, which can set a load of 180 ton on the seabed in 36 m water depth in a high current location in Yell Sound in Shetland (Trapp 2002).

While developing and testing Stingray, EB is also trying to estimate the likely cost of a future tidal farm. The costs involved in the 2002 Stingray program allow them to predict the costs for a 5 MW tidal farm. The value of the power produced by such a farm will be slightly higher than of power delivered by other sources; as the technology of tidal power is developed and refined, the cost of power will be greatly reduced.

8.2. Power generation from currents

The simple theory constructed by Garret & Cummins (2004) emphasizes that power generation by a current cannot occur without the generation of a pressure difference across the turbines, similar to the sea level difference on either side of a water dam. To investigate the power potential of turbines moored across an entrance to a bay, let us use Bernoulli's theorem, which states that in a steady flow of an ideal fluid, the combination of pressure, velocity and gravity force is constant along a given stream-line (cf. Kundu 1990),

$$p/\rho + \frac{u^2 + v^2}{2} + gz = \text{const.} \tag{26}$$

The change in the vertical direction z will be omitted from further considerations.

On the flood-tide, when the flow takes place from the ocean into the bay, the pressure in the entrance in front of turbines is p_0 and the upstream velocity is u_0. Assuming that pressure and velocity along the stream-line which has just passed the row of turbines is p_1 and u_1 (Fig. 20), we can write for the pressure difference across the turbine

$$dp = p_1 - p_0 = \frac{1}{2}\rho(u_0^2 - u_1^2). \tag{27}$$

According to eq. (9) the power generated by this pressure head (per unit area of the turbine) is equal to

$$P = dpu_1 = \frac{1}{2}\rho u_1(u_0^2 - u_1^2). \tag{28}$$

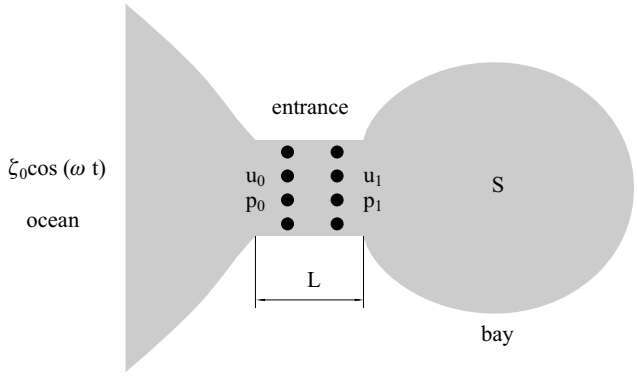

Fig. 20. Diagram of tidal power construction and hydrodynamic modeling in a bay. On the ocean side the tide is described by $\zeta_o \cos(\omega t)$, the dots depict the tidal current generators located in the entrance to the bay

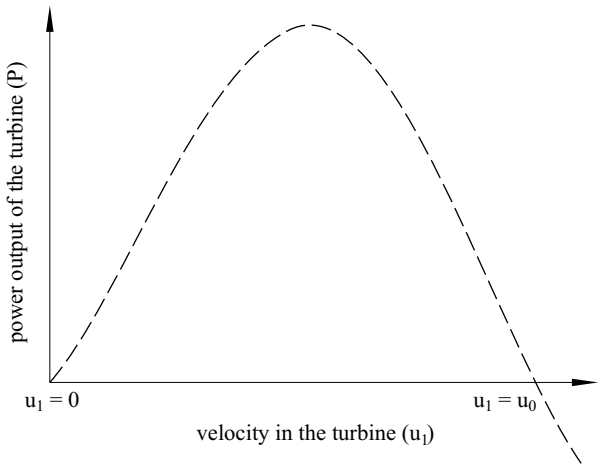

Fig. 21. Power generated by the turbine as a function of the flow velocity u_1 in the turbine

The turbine stops generating power when the velocity diminishes to zero ($u_1 = 0$), and also when the downstream velocity u_1 is greater than the upstream velocity u_0. The behavior of the generated power as a function of a velocity u_1 is clearly illustrated in Fig. 21. The power achieves a maximum at the point where the derivative $\frac{\partial P}{\partial u_1} = 0$

$$\frac{\partial P}{\partial u_1} = \frac{1}{2}\rho(u_0^2 - u_1^2 - 2u_1^2) = 0 \tag{29}$$

or when the flow through the turbine u_1 and in the front of the turbine u_0 are related by $u_1 = \frac{u_0}{\sqrt{3}}$. The maximum power available at this velocity is

$$P_{\max} = \frac{1}{2}\rho\frac{u_0}{\sqrt{3}}(u_0^2 - \frac{u_0^2}{3}) \simeq 0.2\rho u_0^3. \tag{30}$$

This is the upper limit of the power generated per unit (cross-sectional) area of the turbine and it is expressed through the readily available upstream velocity of a free flow u_0 in front of the turbine. It is interesting to note that up to this point we did not mention what kind of fluid is flowing through the turbines. It can be air or water – the difference is in the density. Since the water/air density ratio is approximately 900, the water velocity can be quite small compared to the air velocity needed to achieve the same power.

The dissipated tidal power, defined as the time rate at which work is done by the bottom friction forces (see eq. (18)), is proportional to u^3. As we can glean from the above formula, the available power for electricity generation is also proportional to the velocity cubed. Because of this similarity the exploitation of tidal energy should be directed to reinvesting the dissipated power into the tidal power. Hence, the generation of electricity by tapping kinetic energy may be better tuned to natural dissipation and towards preservation of the natural tidal regime. Unfortunately, the dissipated power is distributed rather smoothly in space, while the tidal energy ought to be tapped in small domains, if it is to be economically viable.

Tidal power tapping by generators moored at the bay entrance leads to a decrease in the flow. Adding more turbines will lead to an even greater change in the tidal pattern. To answer basic questions related to the interactions of the flow and turbines, a simple theory was constucted by Garret & Cummins (2004). A diagram of TPP is given in Fig. 20. The tidal wave elevation in the open ocean is $\zeta_0 \cos(\omega t)$.

The local balance of the forces in the entrance includes the pressure due to the sea slope and the resistance force (F) due to turbines

$$g(Z - \zeta_0 \cos\omega t)/L = -F. \tag{31}$$

Here L denotes the length of the entrance where the turbines are moored. The resistance force is assumed to be a linear function of velocity $F = ru$, and r is the resistance coefficient.

The change in the sea level in the bay is assumed to be uniform over the entire bay; therefore, the continuity equation can be written as (cf. eq. (20))

$$S\frac{\partial Z}{\partial t} = Eu. \tag{32}$$

Here E is the cross-sectional area of the entrance and S is the surface area of the bay. Combining (31) and (32), an equation for the sea level in the bay follows,

$$\frac{\partial Z}{\partial t} + \frac{Eg}{rSL}(Z - \zeta_0 \cos \omega t) = 0. \tag{33}$$

Introducing a new variable $q = Eg/(rSL)$, the above equation is rewritten as

$$\frac{\partial Z}{\partial t} + qZ - q\zeta_0 \cos \omega t = 0, \tag{34}$$

where q denotes the frequency of the natural oscillations in the bay/entrance system. The solution to this nonhomogenous ordinary differential equation can be stated in the form

$$Z = C_1 \sin \omega t + C_2 \cos \omega t. \tag{35}$$

Introducing (35) into (34) and comparing the coefficients of the sin and cos functions, the following expressions are derived for the coefficients,

$$C_1 = \frac{q\omega\zeta_0}{\omega^2 + q^2}; \qquad C_2 = \frac{q^2\zeta_0}{\omega^2 + q^2}. \tag{36}$$

The analytical expression (35) allows us to answer the basic question, namely what will be the sea level change in the bay induced by the turbines located in the entrance. To simplify this solution, two cases can be considered: (a) $\omega \gg q$, and (b) $q \gg \omega$. Thus, the first case assumes that the period of the tide is much shorter than the period of the natural oscillations in the bay/entrance system. Actually, the second case is more realistic, since the tidal period is usually longer than the local period of oscillations. In the second case, the coefficient $C_2 \gg C_1$ and the solution for the sea level simplify to

$$Z \simeq \zeta_0 \cos \omega t. \tag{37}$$

Eq. (37) states an intuitive result, that when the tidal period is much longer than the natural period, the sea level oscillations inside the bay repeat the open ocean tidal oscillations. If such a solution can be achieved through a construction of tidal power generators in the entrance, this will be an important result suggesting that while tidal power is tapped, the tides could be maintained close to the natural regime.

The frequency q can be represented as

$$q = Eg/(rSL) = \omega_H^2/r, \tag{38}$$

where ω_H^2 is the square of the frequency of natural oscillations of the bay. This is called the Helmholtz frequency (Kowalik & Murty 1993, p. 384). The assumption $q \gg \omega$ can be rewritten as

$$\omega_H^2/r \gg \omega \qquad \Rightarrow \qquad \frac{\omega_H^2}{\omega^2} \gg \frac{r}{\omega}. \tag{39}$$

The requirement that $\omega_H^2/r \gg \omega$ is equivalent to the relations between the period of the natural oscillations and the tidal period. The natural oscillations occur for the joint bay/entrance system. The role of the bay's natural oscillations can be investigated through the Helmholtz frequency. It is important to see that the simplified solution derived above is valid only when $q \gg \omega$ is fulfilled. In general, the full solution given by eqs. (35) and (36) should be investigated.

The power gained by the turbines is defined by the time rate at which work is done by the resistance forces averaged over the tidal cycle:

$$P = \rho EL \int_0^T Fu dt. \tag{40}$$

Here $F = ru$, and from eq. (32) u can be calculated as

$$u = \frac{S}{E}\frac{\partial Z}{\partial t}. \tag{41}$$

Introducing the sea level $Z = C_1 \sin\omega t + C_2 \cos\omega t$ from eq. (35), the above velocity is

$$u = \frac{S}{E}(C_1\omega \sin\omega t - C_2\omega \cos\omega t) \tag{42}$$

and the following result is obtained for the power,

$$P = \rho EL\left(\frac{S}{E}\right)^2 r\omega\frac{T}{2}(C_1^2 + C_2^2). \tag{43}$$

The simplified case considered above ($C_2 \gg C_1$) defines $C_2 \simeq \zeta_0 \cos(\omega t)$; therefore the power gained by the turbines is proportional to ζ_0^2 – the square of the amplitude of the tidal wave in the open ocean.

9. Conclusion

Assuming that the total energy produced by work of the Moon and Sun – 4 TW – is dissipated in the World Ocean, the question is how much of this energy can be tapped for electricity generation. At present, the world production of electricity is in the range of 1.5–2 TW. Therefore, at first glance, the available tidal energy seems to be very large. This great amount of energy is distributed over a vast geographical domain. The power available for tapping is probably in the range of 1% to 2% of the total amount, i.e., about 0.04 to 0.08 TW.

This review paper has presented various aspects of tidal power generation. The tapping into the potential and kinetic energy of the tides and the changes that such tapping will introduce in the tidal regime of a small water body connected to the ocean have been considered. The tide in the open ocean was 'given' as a boundary condition. This problem can be extended: we can ask what will happen to the tidal regime in the open ocean when the local potential and kinetic energies start to change? The increased dissipation should lower tidal amplitudes. Therefore, we might ask if there is a limit to the tapping of tidal energy and is it possible that such extraction can lead to change in the tidal dynamics of the Earth-Moon-Sun system.

This is not an easy question to answer, since we are dealing with small (initial) changes in a vast tidal system and dissipation of the tidal energy caused by extraction is not described by the same law as natural dissipation. Therefore, while tidal energy tapping will proceed, it is important to develop a new branch of tidal dynamics which will help to better understand the interaction between the natural tidal regime and future changes that will be introduced by tapping the tidal power. It is especially important to construct tools for evaluating the effect of local changes on the global tidal regime, so that limits to the tidal power extraction could be established. After all, the tidal machine has not only a practical application for delivering tidal power; some of the 4 TW dissipated in the Oceans has relevance for the present and future climate of the earth (Munk & Wunsch 1998).

Acknowledgements

I would like to express my deep gratitude to all who have helped me in my task by offering data, figures and valuable knowledge on tides and tidal energy. I am grateful to: J. Luick, Bill Mitchell and G. Musiela, National Tidal Facility, Adelaide, Australia; R. Flather, Proudman Oceanographic Laboratory, United Kingdom; E. Palma, Universidad Nacional del Sur, Bahía Blanca, Argentina; E. D'Onofrio Departamento Oceanografia, Servicio de Hidrografia Naval, Argentina; A. V. Nekrasov Hydrometeorological

University, St. Petersburg, Russia; C. Garrett, University of Victoria, Victori, Canada; F. Henry and M. Foreman, Institute of Ocean Science, Sidney, Canada; H. Mofjeld, PMEL, Seattle, A. Proshutinsky, WHOI, and C. Lomax, The Engineering Business Ltd.

References

Bernshtein L. B., 1961, *Tidal energy for electric power plants*, Israel Program for Scientific Translations, Jerusalem, 378 pp.

Bernshtein L. B. (ed.), 1996, *Tidal power plants*, Korea Ocean Res. & Development Institute, Seoul, 444 pp.

Cartwright D. E., 1969, *Extraordinary tidal currents near St. Kilda*, Nature, 223, 928–932.

Defant A., 1960, *Physical oceanography*, Vol. 2, Pergamon Press, New York, 598 pp.

Egbert G. D., Ray R. D., 2000, *Significant dissipation of tidal energy in the deep ocean inferred from satellite altimeter data*, Nature, 405, 775–778.

Flather R. A., 1976, *A tidal model of the north-west European continental shelf*, Mem. Soc. Roy. Sci. Liege, 6 (10), 141–164.

Garrett C., 1984, *Tides and tidal power in the Bay of Fundy*, Endeavour, New Ser., 8 (2), 160–167.

Garrett C., Cummins P., 2004, *Generating tidal power from currents*, J. Waterw. Port C-ASCE, 130 (3), 114–118.

Garrett C., Greenberg D. A., 1977, *Predicting changes in tidal regime: The open boundary problem*, J. Phys. Oceanogr., 7, 171–181.

Gibrat R., 1966, *L'energie des marees*, Presses Univ. France, Paris, 219 pp.

Glorioso P. D., Flather R. A., 1997, *The Patagonian Shelf tides*, Prog. Oceanogr., 40, 263–283.

Godin G., 1988, *Tides*, CICESE, Ensenada Baja California, 290 pp.

Gorlov A. M., 2001, *Tidal energy*, [in:] *Encyclopedia of ocean sciences*, Acad. Press, London, 2955–2960.

Greenberg D. A., 1979, *A numerical model investigation of tidal phenomena in the Bay of Fundy and Gulf of Maine*, Mar. Geod., 2 (2), 161–187.

Henry R. F., Foreman M. G. G., 2001, *A representation of tidal currents based on energy flux*, Mar. Geod., 2493, 139–152.

Holloway P. E., 1987, *Internal hydraulic jumps and solitons at a shelf break region on the Australian North West Shelf*, J. Geophys. Res., 92 (C5), 5405–5416.

Kagan B. A., 1997, *Earth–Moon tidal evolution: model results and observational evidence*, Prog. Oceanogr., 40, 109–124.

Kantha L. H., 1995, *Barotropic tides in the global oceans from a nonlinear tidal model assimilating altimetric tides. 1. Model description and results*, J. Geophys. Res., 100, 25,283–25,308.

Kantha L. H., Clayson C. A., 2000, *Numerical models of oceans and oceanic processes*, Acad. Press, San Diego, 940 pp.

Kowalik Z., Murty T. S., 1993, *Numerical modeling of ocean dynamics*, World Sci. Publ., Singapore, 481 pp.

Kowalik Z., Polyakov I., 1998, *Tides in the Sea of Okhotsk*, J. Phys. Oceanogr., 28 (7), 1389–1409.

Kowalik Z., Proshutinsky A. Yu., 1993, *Diurnal tides in the Arctic Ocean*, J. Geophys. Res., 98, 16449–16468.

Kundu P., 1990, *Fluid dynamics*, Acad. Press, New York, 638 pp.

Lawton F. L., 1972. *Economics of tidal power*, [in:] *Tidal power*, T. J. Gray & O. K. Gashus (eds.), Plennum Press, New York, 105–130.

LeBlond P. H., Mysak L. A., 1978, *Waves in the ocean*, Elsevier, Amsterdam, 602 pp.

LeProvost C., Genco M. L., Lyard F., 1994, *Spectroscopy of the world ocean tides from a finite element hydrodynamic model*, J. Geophys. Res., 99, 24,777–24,797.

LeProvost C., Lyard F., 1997, *Energetics of the M_2 barotropic ocean tides: an estimate of bottom friction dissipation from a hydrodynamic model*, Prog. Oceanogr., 40, 37–52.

Munk W., 1997, *Once again: once again–tidal friction*, Prog. Oceanogr., 40, 7–35.

Munk W. H., Wunsch C., 1998, *Abyssal recipes II: Energetics of tidal and wind mixing*, Deep-Sea Res., 45, 1977–2010.

Nekrasov A. V., 1990, *Energy of ocean tides*, Gidrometeoizdat, Leningrad, 288 pp.

Nekrasov A. V., 1992, *On tidal energy horizontal circulation*, J. Korean Soc. Coast. Ocean Eng., 4 (3), 168–177.

NTF Australia, 2000, *Western Australian sea level variability due to tides, weather and extreme events*, A report to The Government of Western Australia, Coastal Management Branch, Department of Transport, National Tidal Facility Australia, Adelaide, 46 pp.

Palma E. D., Matano R. P., Piola A. R., *A numerical study of the Southwestern Atlantic Shelf circulation. Part I: The barotropic response to tidal and wind forcing*, J. Geophys. Res.-Oceans, (in press).

Patchen R. C., Bruce J. T., Connolly M. J., 1981, *Cook Inlet circulatory survey: 1973–75*, NOS Oceanographic Circulatory Survey Rep. No 4, Rockville, Md., 89 pp.

Pelletier R. R., McMullen R. M., 1972, *Sedimentation patterns in the Bay of Fundy and Minas Basin*, [in:] *Tidal power*, T. J. Gray & O. K. Gashus (eds.), Plennum Press, New York, 153–188.

Prandle D., 1984, *Simple theory for designing tidal power schemes*, Adv. Water Resour., 7, 12–27.

Pugh D. T., 1987 *Tides, surges and mean sea-level*, John Wiley & Sons, Chichester, 472 pp.

Shum C. K., et al., 1997, *Accuracy assessment of recent ocean models*, J. Geophys. Res., 102, 25,173–25,194.

Stone R., 2003, *Norway goes with the flow to light up its nights*, Science, 299, p. 399.

Taylor G. I., 1921. *Tidal oscillations in gulfs and rectangular basins*, Proc. Lond. Math. Soc. (2nd ser.), 20, 148–181.

Trapp T., 2002, *The Stingray programme 2002*, The Engineering Business Ltd., M02–151–01.doc, 4 pp.

Trapp T., Watchorn M., 2001, *EB development of tidal stream energy*, The Institute of Marine Engineers, MAREC 2001 Conf., The Engineering Business Ltd. (http://www.engb.com), 6 pp.

United States Coastal Pilot, 1995, *Pacific and Arctic Coasts of Alaska*, NOAA, Washington, DC, 334 pp.

Wunsch C., 1975, *Internal tides in the ocean*, Rev. Geophys. Space Phys., 13, 167–182.